Received: November 2, 2023. Revised: December 2, 2023.

INASS

International Journal of
Intelligent Engineering & Systems

http://www.inass.org/

Design and Optimization of Hybrid Precoders in Massive MIMO Systems: Leveraging Low-Resolution ADCs/DACs, Reconfigurable Intelligent Surfaces, and Deep Learning Algorithms

Girish Kumar N G[1]* **M N Sree Ranga Raju[2]**

[1]*Department of Electronics and Telecommunication, Bangalore Institute of Technology, India*
[2]*Department of Electronics and Communication, Bangalore Institute of Technology, India*
* Corresponding author's Email: girishkumarng@bit-bangalore.edu.in

Abstract: In this research, we propose an advanced hybrid precoding design for massive MIMO systems. Our approach integrates two innovative strategies: employing low-resolution ADCs and DACs with non-uniform quantization (NniQ) and implementing dynamic hybrid relay reconfigurable intelligent surfaces (DHRR-RIS). We utilize an iterative alternating minimization algorithm to improve spectral and energy efficiency in the first strategy. The second approach integrates DHRR-RIS with machine learning techniques, including adaptive back propagation neural network (ABPNN) for channel estimation, deep deterministic policy gradient (DDPG) algorithm for hybrid precoding and combining, fire hawk optimization (FHO) for DHRR-RIS, and enhanced fuzzy C-means (EFCM) for data clustering. These methodologies significantly enhance bit error rate (BER) and weighted sum rate (WSR) compared to traditional uniform quantization (UniQ) methods. Our results show that combining low-resolution ADCs/DACs with NniQ and DHRR-RIS, further optimized by machine learning, effectively reduces hardware complexity and power usage while markedly improving BER and WSR, offering a promising direction for efficient massive MIMO system development.

Keywords: Low-resolution DACs/ADCs, Quantization, Hybrid precoder, Reconfigurable intelligent surfaces, Machine learning and deep learning algorithms, Massive MIMO systems.

1. Introduction

Massive multiple-input, multiple-output (MIMO) technology has become a cornerstone for next-generation wireless communication networks. The ability of these systems to transmit and receive multiple data streams simultaneously enables high SE, low latency, and robust communications, meeting the demands of societal needs [1]. However, the implementation of massive MIMO systems as shown in Fig. 1 faces significant challenges, particularly in the design of efficient hybrid precoders.

Traditionally, fully digital precoding techniques have been employed to optimize the performance of massive MIMO systems [2]. However, these approaches often require high-resolution ADCs/DACs, leading to increased hardware complexity and power consumption [3, 4]. We employed a low-resolution ADCs/DACs with NUQ and iterative alternating minimization algorithm to achieve a fine balance between SE and EE, thereby reducing both hardware complexity and power consumption. Additionally, RIS are introduced as a potential solution to some inherent challenges in massive MIMO systems. RIS, involving smart surfaces capable of controllable passive reflection of electromagnetic waves, can significantly enhance the wireless communication landscape [5, 6]. Our research further incorporates DHRR-RIS alongside 4-bit ADCs/DACs.

We employed machine learning algorithms, namely the ABPNN for pilot and channel state information (CSI) optimization, the DDPG for hybrid precoder optimization at the base station (BS), and the FHO algorithm for DHRR-RIS configuration,

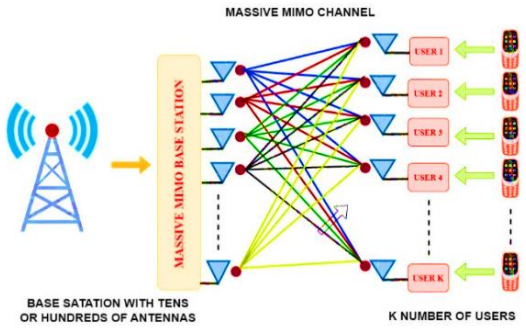

Figure. 1 Block diagram of massive MIMO system

Table 1. Notations

Notation	Description
NniQ	Non-Uniform Quantization
UniQ	Uniform Quantization
q	DAC Resolution
b	ADC Resolution
x	Transmitted Data
y	Received data
$Q_{NniQ(D)}$	Non-Uniform Quantization Process
P	Transmitter Power
b	Distortion factor of DAC
τ	Total Reflection Coefficient
γ	Total Reflection Coefficient Matrix
α	Passive element coefficient Matrix
S	Transmitted Signal vector
ω	Channel Gain
N_{BS}, M_{BS}	Number of Base Station Antennas
N_{UT}, M_{UT}	Number of receiving antennas
a	Distortion induced by ADC
H	Channel Matrix
β	Active element coefficient Matrix
$\mathbb{C}$	Complex Number
MSE	Mean Square Error
B	Bandwidth
F	Product of Analog and Digital precoder Matrices

aiming to improve performance metrics such as WSR and BER. The objective of this paper is to integrate these technological advancements in the design and optimization of hybrid precoders for massive MIMO systems, presenting a holistic approach to address current challenges in the field.

The paper is organized as follows: Section 2 offers a literature review, section 3 delineates the research contributions, section 4 describes the system model for hybrid precoding in massive MIMO systems, section 5 discusses problem formulation, section 6 presents simulation results, section 7 analyses computational complexity, and section 8 concludes the study.

2. Literature review

This literature review embarks on a meticulous exploration of prevailing research, systematically dissecting the various techniques and methodologies adopted by scholars in these realms.

2.1 Quantization techniques in massive MIMO and mmWave systems

This review delves into research on hybrid precoding, mmWave channels, expansive MIMO systems, and low-resolution ADCs and DACs, aiming to critically analyse their methodologies, strengths, and weaknesses, especially in the context of uniform and NniQ strategies. A notable observation is the limited research on NUQ's role with low-resolution ADCs/DACs, suggesting potential areas for system improvement.

[7] discussed hybrid precoding in mmWave channels with a partially connected setup, while reducing hardware complexity, faces challenges in beamforming flexibility and spatial multiplexing capabilities The adaptation of DFT codebooks by the statistical correlation matrix may not always align with RF hardware constraints, necessitating additional processing like phase extraction techniques.[8] introduced a DFT codebook-based hybrid precoding for multiuser mmWave massive MIMO. This work depends on accurate CSI. [9] proposed a hybrid precoding method for massive MIMO systems with low-rank channels. But Due to the reduced rank of the channel matrix, the number of effectively distinguishable paths for data transmission is limited. [10] compared hybrid and full-digital beamforming in mmWave massive MIMO systems with low-resolution ADCs. Purely Worked on UniQ and not considered NniQ. [11] contributed to achievable rates for full-duplex massive MIMO with low-resolution ADCs/DACs, focusing on system performance. In contrast, our study provides a comprehensive evaluation incorporating quantization error, interference types, and highlights the advantages of power scaling and ADC/DAC resolution adjustments, emphasizing the relevance of low-resolution ADCs/DACs in FD massive MIMO systems.

[12] investigated full-duplex massive MIMO systems with low-resolution ADCs/DACs. Further studies, such as those by [13-15], delved into various massive MIMO system aspects using low-resolution ADCs/DACs. [16] studied SE and EE optimization with low-precision ADCs. [17-19] examined secure transmission, downlink D2D analysis, and indoor

THz systems, respectively Specific to one-bit DACs. [20-22] investigated full-duplex massive MIMO cellular networks, multicast downlink, and mmWave systems, respectively. [23] focused on low-resolution ADC massive MIMO systems, emphasizing achievable rates and bit allocation. study in [24] introduced a learning-based method for one-bit ADCs in massive MIMO systems. [25] addressed the challenges in massive MIMO systems concerning low-resolution DACs and proposed a 1-bit downlink precoding algorithm with Inherent complexity, NP-hard problem.

Despite these insights, the benefits of NniQ remain unexplored. Introducing NniQ may offer enhanced noise reduction, improving SE and EE, potential hardware simplification and reduced power consumption due to optimized ADC/DAC resolution use.

Our study aims in providing a comprehensive evaluation of quantization error and the advantages of power scaling in low-resolution ADCs/DACs systems. We identify the need for advanced quantization techniques that can optimize SE and EE, proposing NniQ as a solution to achieve noise reduction, hardware simplification, and reduced power consumption.

2.2 RIS-assisted channel estimation & hybrid precoder design using machine learning algorithms

In [26], a methodology employing deep learning for hybrid precoding in MIMO-oriented THz communication via RIS is put forward, wherein a phased array analog precoder is supplanted with RIS and analog beamforming is optimized via a concurrent deep neural network. Digital precoding optimization employs zero-forcing algorithms, but this work relies on sophisticated control for active elements and so power consumption. [27] presents a hybrid precoding structure for MIMO systems employing dual RIS, optimizing digital and analog precoders collectively at the transmitter and RIS through quadratically constrained quadratic programming and riemannian optimization algorithms, respectively but dependent on accurate CSI. [28] features hybrid precoder design using a deep reinforcement learning algorithm for THz communication, with the optimized policy embodying the digital and analog precoder optimization actions of the THz system, but dependent on accurate CSI.

In [29], a machine learning algorithm is utilized for channel estimation in wireless communication, employing a distributed machine learning algorithm to augment reliability. Here significant computational resources are required for implementing DRL. [30] designs the hybrid precoder using RIS for MIMO systems with fixed precoders employing EMser and VGMser reflection methods. [31] introduces the design of robust hybrid precoders by concurrently estimating the channel state and optimizing the RIS reflecting element. But still dependency on accurate CSI. Finally, [32] employs adaptive resolution analog to digital converters for RIS-based MIMO systems, achieving robust, energy-efficient hybrid beamforming through joint optimization of the converter resolution, RIS power, and reflecting element positioning but assumes infinite phase resolution and known CSI.

Building on the foundations laid by studies [26-32], our research further explores the integration of RIS with machine learning algorithms for channel estimation and hybrid precoder design. Previous research, such as [26, 27], has introduced methodologies for optimizing digital and analog precoders using deep learning and advanced optimization algorithms.

However, these studies often lack a holistic approach in optimizing the entire system, including RIS elements, for achieving maximum efficiency. Our work extends these concepts by employing adaptive resolution ADCs in RIS-based MIMO systems, as proposed in [32], and focuses on joint optimization strategies that encompass converter resolution, RIS power, and element positioning, thereby aiming for a more robust and energy-efficient system.

2.3 Designing hybrid precoders without RIS and using machine learning algorithms

In [33], deep learning-driven hybrid precoding for MIMO systems involves training pilot signals, with estimations on both short and long temporal scales. [34] presents a deep learning-based hybrid precoding for MIMO, leveraging convolutional neural networks and deep neural networks for channel state estimation. [35] introduces a deep convolutional neural network-based framework for mmWave MIMO systems, optimizing radio frequency chains and boosting SE. [36] describes a machine learning hybrid precoding for multi-user MIMO systems, integrating the Dinkelbach and water-filling algorithms for optimization.

In [37], a deep learning technique is employed for hybrid precoding in mmWave massive MIMO systems, using neural networks and zero-forcing algorithms. [38] offers a similar deep learning-based approach for time division duplexing massive MIMO

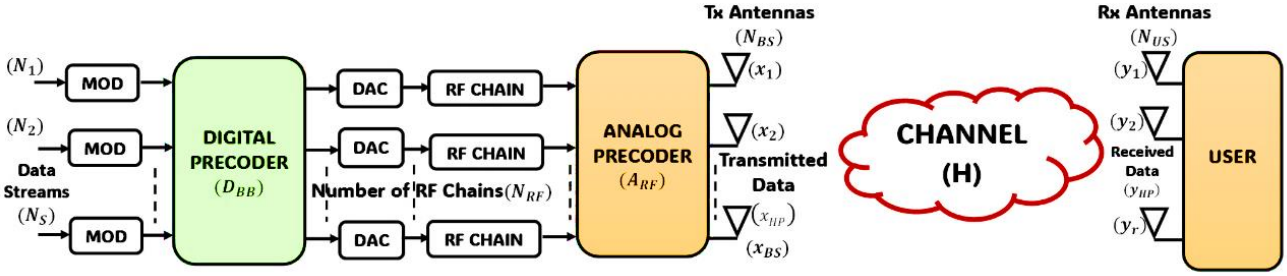

Figure. 2 Block diagram of hybrid precoder for conventional massive MIMO system

systems, focusing on reducing overhead.

[39] uses a deep learning algorithm for hybrid precoding in mmWave massive MIMO systems, enhancing SE and robustness. [40] optimizes MIMO channel estimation using lower resolution converters, showing reduced hardware and power requirements. A cross-entropy-based machine learning approach for hybrid precoding is highlighted in [41]. [42] explores channel estimation in massive MIMO systems via deep learning, combining a deep neural network with a fuzzy c-means clustering algorithm. [43] proposes a low-complexity deep learning precoding algorithm for MIMO systems, optimizing user quality of service. [44] introduces a deep reinforcement learning approach for mmWave hybrid precoders, while [45] presents a distributed neural precoding technique for mmWave MIMO systems, underlining significant performance enhancements.

In the realm of hybrid precoding without RIS, studies [33-45] have made significant strides in employing deep learning for system optimization.

While these studies have contributed valuable insights, especially in enhancing SE and reducing system complexity, they often overlook the potential synergies between low-resolution ADCs/DACs and machine learning algorithms. Our work seeks to bridge this gap by leveraging deep learning algorithms for optimizing hybrid precoders in massive MIMO systems with low-resolution converters. This approach promises to reduce hardware and power requirements significantly, while enhancing overall system performance.

3. Research contributions

In our work we address some of the challenges to enhance performance of massive MIMO systems by:

- **Efficiency optimization:** Examining the trade-offs of SE and EE by deploying varied resolution DACs and ADCs, thereby addressing the consequential power implications at the base station.
- **Quantization analysis:** Utilizing UniQ and NniQ quantization techniques, we elucidate SE metrics and subsequently devise a novel algorithm for NniQ, targeting performance enhancements in massive MIMO systems with constrained ADCs/DACs resolutions.
- **Precoder design with and without using machine learning approaches:** Using alternating minimization, we've crafted precoding techniques without machine learning, targeting performance akin to UniQ and NniQ DACs and ADCs systems. Furthermore, by blending DDPG for digital and analog precoding with FHO for DHRR-RIS and ABPNN for channel estimation, we've devised a hybrid precoding approach for improved communication efficiency.
- **Simulation:** MATLAB R2023a simulations are employed to benchmark our innovations against prevailing models, underscoring the transformative potential of integrating machine learning algorithms and DHRR-RIS in massive MIMO systems.

Collectively, this research seeks to foster innovative paradigms in massive MIMO systems, amalgamating foundational concepts with emerging technologies.

4. System model

In this paper, we investigate the design of hybrid precoders for massive MIMO systems in two different scenarios: a conventional massive MIMO system and a massive MIMO system enhanced by a DHRR-RIS. The overarching objective is to analyse and optimize the performance of low-resolution ADCs and DACs within these architectures, leveraging both machine learning and deep learning algorithms.

4.1 System model of NniQ and UniQ massive MIMO system

In the conventional setup, we consider a single-user point-to-point massive MIMO system consisting

of transmitter antennas at the base station (BS) and receiver antennas at the User (UT) as shown in Fig. 2. The baseband and RF precoding matrices are denoted by $D_{BB} \in \mathbb{C}^{N_{RF} \times N_S}$ and $A_{RF} \in \mathbb{C}^{N_{BS} \times N_{RF}}$, where N_{RF} is the number of RF chains and N_S is the number of streams. The transmitted vector $x_{HP} \in \mathbb{C}^{N_{BS} \times 1}$ from the BS is obtained using hybrid precoding as:

$$x_{HP} = \sqrt{P} A_{RF} Q_{NniQ(D)}(D_{BB} \times S) \quad (1)$$

Where $Q_{NniQ}(.)$ is the NniQ process of DAC, S is a transmitted signal vector, P is the transmitter power, A_{RF} is the analog precoder matrix and D_{BB} is the digital precoder matrix. After multipath fading, the received vector $y_{HP} \in \mathbb{C}^{N_{US} \times 1}$ at the UT is:

$$y_{HP} = H x_{HP} + n \quad (2)$$

Where $H \in \mathbb{C}^{N_{UT} \times N_{BS}}$ is the channel matrix and n is the additive white Gaussian i.i.d noise with zero mean and variance. Here channel state information (CSI) is assumed to be known at both the BS and US [3]. In the first scenario, The saleh-valenzuela (SV) channel model [3] has been used considering 6 clusters, with each cluster containing 8 rays. This specific configuration was chosen to model indoor environments where multipath components are abundant. Mathematically the channel response vector is obtained by:

$$h_{HP} = \sqrt{\frac{N_{BS} N_{UT}}{Q}} \sum_{q=1}^{Q} \omega_l f_{UT}(\varphi) {f_{BS}}^{H}(\varphi) \quad (3)$$

where ω_l is the channel gain of the path l, $f_{US}(\varphi)$ and $f_{BS}(\varphi)$ are the channel array response vectors of the User Terminal and Base station respectively. Here uniform linear array (ULA) is considered and so the channel vectors are independent of elevation angle. The channel array response vectors at both the base station and user terminal are given by:

$$f_{US,BS}(\varphi) = \frac{1}{\sqrt{N}} \left[1, e^{\frac{i2\pi}{\lambda} d sin(\varphi)}, .., e^{\frac{i2\pi}{\lambda} d(N-1) sin(\varphi)}\right]^T \quad (4)$$

Where N is the total number of elements in an array, φ is the azimuth angle between $[0,2\pi)$, d is the antenna spacing and λ is the wavelength.

The received vector y at the receiver undergoes NniQ at ADC, this is formulated as:

$$f = Q_{NniQ(A)}(H x_{HP} + n) \quad (5)$$

By considering buss gang theorem and additive quantization noise model (AQNM) [3], the received vector after NniQ is given by:

$$f = (1-a)(1-b)\sqrt{P} A_{RF} D_{BB} S + (1-a)\sqrt{P} H A_{RF} u + (1-a) n + r \quad (6)$$

Where b is the distortion factor of DAC,a is the distortion induced by ADC, u is the uncorrelated quantization error of DAC, and r is the ADC distortion. Contrary to UniQ which is governed by the minimum value of x_{HP}, NniQ is influenced by the maximum value of x_{HP}. Given the nonlinear relation between quantized and unquantized values in NniQ, there's an opportunity to minimize distortion. To exploit this relationship, we developed a custom NniQ equation, capturing the essence of Precoded symbol dependencies:

$$x_i^{qua} = \left\lfloor \left(\frac{x_i(2^{qua}-1)}{(2^{qua}-1)}\right) \times sign(x_i) \times \left(\frac{x_{max}-x_{min}}{2^{qua}+1}\right) + 0.5 \right\rfloor \quad (7)$$

This custom NniQ is designed to offer enhanced representation efficiency for our application. In the above equation, the operator $\lfloor . \rfloor$ is the round-off operator, x_{max}, x_{min} maximum and minimum value of user precoded symbols and ${x_i}^{qua}$ stands for quantized data.

4.2 System model of DHRR-RIS based massive MIMO system

The second scenario introduces a DHRR-RIS between the BS and the UE to facilitate downlink data transmission, especially when direct links are hindered by blockages or path loss as shown in Fig. 3.

DHRR-RIS is a design addressing conventional RIS limitations, specifically in CSI acquisition and phase control. Its elements, both passive (V) and active (L), are represented as $M = L + V$ where $1 \leq L \ll V$ and M is the total number of DHRR RIS elements [27]. The passive components, serving as analog beamformers, use vector modulated phase shifters to guide beams. On the contrary, active components handle separate channel state estimations for both transmitter and receiver. Let us consider $B \subseteq \{1,2,\ldots,M\}$ which is a set of position of L active elements. The reflection/relay coefficient $\tau_k$is given by:

$$\tau_k = \begin{cases} |\tau_k| e^{j\emptyset_k}, \ if \ k \in B \\ e^{j\emptyset_k}, \ otherwise \end{cases} \quad (8)$$

Where $\emptyset_k \in [0,2\pi)$ represents the phase shift.

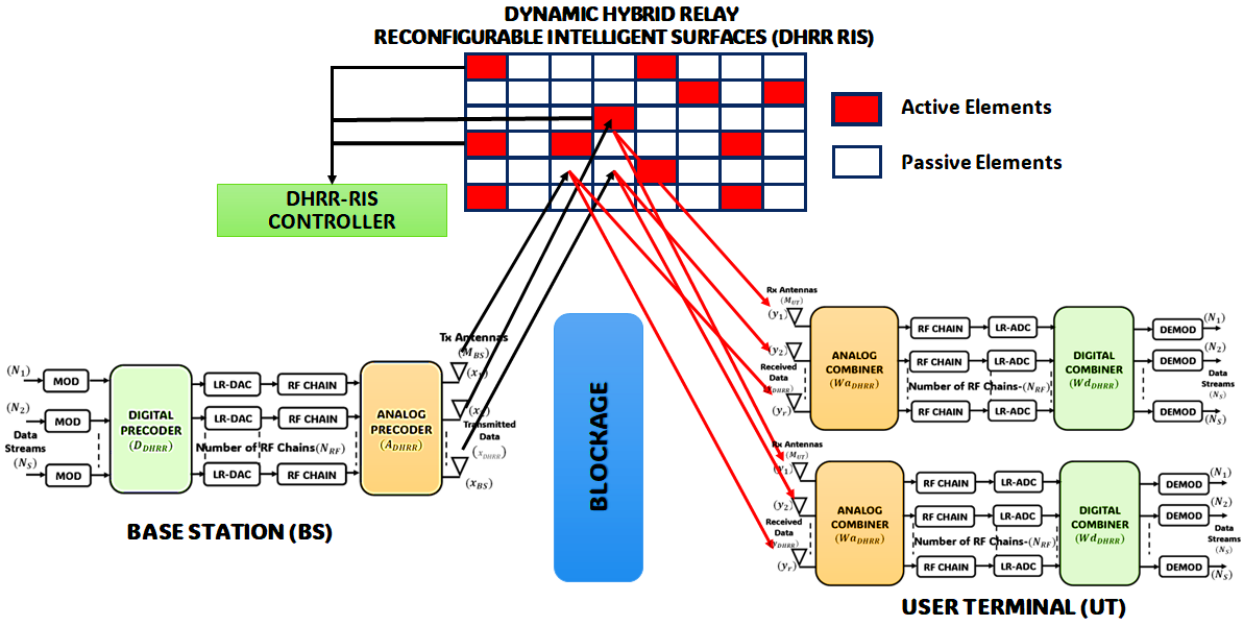

Figure. 3 Block diagram of hybrid precoder and combiner for massive MIMO system using DHRR-RIS

We also consider three diagonal matrices based on τ_k. $\gamma = diag(\tau_1, \tau_2, \dots\dots, \tau_M)$, $\alpha = \{\alpha_1, \alpha_2, \dots\dots, \alpha_M\}$ and $\beta = \{\beta_1, \beta_2, \dots\dots, \beta_M\}$.

$$\alpha_k = \begin{cases} 0, \ if \ k \in B \\ \tau_k, \ otherwise \end{cases} \quad (9)$$

$$\beta_k = \begin{cases} \tau_k, \ if \ k \in B \\ 0, \ otherwise \end{cases} \quad (10)$$

Where α and β contain only the passive and active relaying coefficients, respectively, while γ contains the coefficient of all elements of DHRR-RIS. Therefore, $\gamma = \alpha + \beta$. We also note that $|\tau_k| = 1 \ for \ all \ k \notin$ B.

We denote the channel between the BS and DHRR-RIS by $H_t \in \mathbb{C}^{M \times M_{BS}}$ and the channel between the DHRR-RIS and the UE by $H_r \in \mathbb{C}^{M_{UT} \times M}$. Where M_{BS} is total number of base station antennas and M_{UT} are the total number of antennas at the User Terminal. The transmission signal vector can be represented as $y_{DHRR} \in \mathbb{C}^{M_{UT} \times 1}$. M is the total number of elements in DHRR-RIS. During transmission digital or baseband precoding is applied at the base station for data streams followed by analog precoding. The received signal at the UT in the presence of DHRR-RIS can be expressed as:

$$y_{DHRR} = H_r \alpha H_t x_{DHRR} + H_r \beta H_t x_{DHRR} + H_r \beta N_H + n_{UT} \quad (11)$$

$$y_{DHRR} = (H_r \alpha H_t + H_r \beta H_t) x_{DHRR} + n_{DHRR} \quad (12)$$

$$y_{DHRR} = H_r \gamma H_t x_{DHRR} + n_{DHRR} \quad (13)$$

Where $N_H \sim CN(0, \sigma_H^2 I_L)$ is the complex Gaussian noise vectors due to active relay elements at DHRR RIS and $n_{UT} \sim CN(0, \sigma_{UT}^2 I_{N_{UT}})$ is the complex Gaussian noise vectors due to M_{UT} receiver antennas. For simplicity we assume $\sigma_H^2 = \sigma_{UT}^2 = \sigma^2$ and $N \sim CN\left(0, \sigma^2\left(I_{M_{UT}} + H_r \beta\beta^H H_r^H\right)\right)$. The x_{DHRR} is the transmitter vector from the base station. In this work same Saleh Valenzuela channel model [3] is used to generate the channel matrix H, were all three components, base station, User Terminal and DHRR RIS antenna elements are Uniform Planar array (UPA) [27].

So, the channel response vector is obtained by,

$$H_{n,m} = \sqrt{\frac{N_{DHRR}}{Q_{DHRR}}} \sum_{q=1}^{Q_{DHRR}} \omega_{n,m}^{(q)} f_{DHRR}\left(\varphi_{n,m}^{(q)}, \theta_{n,m}^{(q)}\right) \quad (14)$$

Here, Q_{DHRR} is the number of multipath components between sub surface of DHRR-RIS and UT, N_{DHRR} is the number of elements in the DHRR-RIS, and $\omega, \varphi_{n,m}^{(q)}, \theta_{n,m}^{(q)}$ are the antenna gain, azimuth and elevation angles of departure (AoD) of the path, respectively. DHRR RIS antenna's structure ($M = M_{m1} \times M_{m2}$) is considered in which horizontal direction M_{m1} and vertical direction M_{m2} antenna elements are considered. The total array response vector is formulated as:

$$f_{DHRR}(\varphi, \theta) = f_{DHRR_{azi}}(\varphi) \otimes f_{DHRR_{ele}}(\theta) \quad (15)$$

Where, the $f_{DHRR_{azi}}(\varphi)$ and $f_{DHRR_{ele}}(\theta)$ can be expanded as,

$$f_{DHRR_{azi}}(\varphi) = \frac{1}{\sqrt{M_{m1}}}\left[e^{i2\pi i\left(\frac{d_1}{\lambda}\right)\sin(\varphi)}\right]^T, \quad i \in I(M_{m1}) \quad (16)$$

$$f_{DHRR_{ele}}(\theta) = \frac{1}{\sqrt{M_{m2}}}\left[e^{j2\pi j\left(\frac{d_2}{\lambda}\right)\sin(\theta)}\right]^T, \quad j \in I(M_{m2}) \quad (17)$$

Where λ is the wavelength, d_1 is the antenna spacing in horizontal direction, d_2 is the antenna spacing in vertical direction, and $I(n) = \{0,1, \dots \dots \dots, n-1\}$.

5. Problem formulation

The primary objective of this work is twofold. First, it seeks to enhance the SE and EE of massive MIMO systems equipped with low resolution DACs/ADCs, specifically in single-user scenarios. Secondly, in multi-user cases involving DHRR RIS-based massive MIMO, the focus shifts to optimizing the WSR and BER. Both pursuits aim for optimal system performance.

5.1 Problem formulation for single-user massive MIMO systems

5.1.1. Maximize SE

Mathematically, this can be represented as:
Objective function:

$$SE = log_2\left|I_{N_r} + \frac{R_{\hat{S}\hat{S}}}{R_{\hat{u}\hat{u}}+R_{\hat{n}\hat{n}}+R_{\hat{r}\hat{r}}}\right| \quad (18)$$

$$SE = log_2\left|I_{N_{UT}} + b\frac{P}{N_s}(R_n)^{-1}HA_{RF}D_{BB}{D_{BB}}^H{A_{RF}}^H H^H\right| \quad (19)$$

Constraints:

- $R_{\hat{S}\hat{S}}$ is covariance matrix of required signal.
- $R_{\hat{u}\hat{u}}$ is covariance matrix of DAC distortion.
- $R_{\hat{n}\hat{n}}$ is covariance matrix of white noise.
- $R_{\hat{r}\hat{r}}$ is covariance matrix of ADC distortion.

5.1.2. Maximize EE

Mathematically, this can be represented as:
Objective function:

$$EE = \frac{B\times SE}{P_{tot}} \quad (20)$$

Table 1. Power consumption by each device [3]

Device	Notation	Values
Local Oscillator	P_{LO}	22.5mW
Hybrid with buffer	P_{HB}	3mW
Power Amplifier	P_{PA}	P/0.25
Low Pass Filter	P_{LF}	14mW
Mixer	P_M	0.3mW
Phase Shifter	P_{PS}	21.6mW

Algorithm 1	**Iterative Alternating Minimization Algorithm for Precoder Design**
input	$H, N_{RF}, N_S,$ Number of Iterations (i)
output	Analog Precoder Matrix A_{RF} Digital Precoder Matrix D_{BB}
initially	$[:,:,v^H] = SVD(H)$, $(v^H)' = W_{opt}$
then	Calculate $\hat{A} = e^{\angle[rand(N_t,N_r)}$ with random phases
for	$1 \le i \le I\ do$
	Stage 1: Fix $\hat{A}$, calculate $\widehat{D} = (\hat{A})^H W_{opt}$
	Calculate $F = W_{opt}(\widehat{D})^H$
	Stage 2: Fix $\widehat{D}$, update $\hat{A}, \hat{A} = e^{\angle\lvert F\rvert}$
end for	
finally,	$A_{RF} = \hat{A},\ D_{BB} = \sqrt{N_S}\frac{\widehat{D}}{\lVert A\widehat{D}\rVert_F}$

Constraints:

$$P_{tot} = P_{LO} + P_{PA} + 2N_rP_{ADC} + N_{RF}N_tP_{ps} + N_{RF}(2P_{DAC} + P_{RF}) \quad (21)$$

$$P_{RF} = 2P_M + 2P_{LF} + P_{HB}, P_{DAC} = c_1f_1q + c_2 2^q \text{ and } P_{ADC} = jf_r2^b \quad (22)$$

5.1.3. Hybrid precoder design

An iterative alternating minimization algorithm 1 [3] is used to optimize the hybrid precoder, thereby achieving the maximization of both SE and EE under the given constraints.

5.2 Problem formulation for massive MIMO systems using DHRR-RIS

Given a massive MIMO system employing a hybrid precoder with DHRR-RIS, we seek to optimize the system's performance in terms of the WSR, BER and SE.

5.2.1. Maximizing achievable WSR

When a multiuser scenario is considered the weighted sum rate WSR is formulated as:

$$WSR = \sum_{i=1}^{K} W_i log_2(1 + SINR_i(A_{DHRR}, D_{DHRR}, \gamma) \quad (23)$$

Where $SINR_i$ is the signal to interference noise ratio of the i^{th} user and W_i is the weight assigned to the i^{th} user and K is the total number of users. $\boldsymbol{\gamma}$ is the reflection coefficient of DHRR-RIS.

$$SINR_i = \frac{|{H_i}^H A_{DHRR} \gamma {D_{DHRR}}^i|}{\sum_{i' \neq i}^{K} |{H_i}^H A_{DHRR} \gamma {D_{DHRR}}^{i'}| + \sigma^2} \quad (24)$$

Where H_i is the channel matrix of i^{th} user, A_{DHRR} and D_{DHRR} are the analog and digital precoder matrices obtained through DDPG algorithm respectively. σ^2 is variance of AWGN.

Objective function:

$$\left({A_{DHRR}}^{\text{opt}}, {D_{DHRR}}^{\text{opt}}\right) = \arg\max_{\text{b,pre}} (WSR) \quad (25)$$
$$\text{Subject to, } c_1: \|D_{DHRR}\|_D^2 \leq P_t$$
$$c_2: D_{DHRR} \in \zeta$$

Where $\boldsymbol{P_t}$ is maximum transmission power and $\boldsymbol{\zeta}$ is the set of all possible Analog beamforming matrices.

5.2.2. Minimizing BER

BER is pivotal in gauging the reliability of massive MIMO systems, particularly when employing advanced hybrid precoding designs integrated with DHRR-RIS. We utilize the Saleh-Valenzuela (S-V) channel model, ensuring a realistic portrayal of massive MIMO propagation characteristics. The core system optimizations come from the interplay between the DDPG for precoding, Fire Hawk optimization for DHRR-RIS, ABPNN for CSI estimation, and the EFCM algorithm for data stream clustering. For our M-QAM modulated system, the BER, influenced by the SINR, is approximated by:

$$BER_{DHRR} \approx \frac{4}{\log_2 M} erfc\left(\sqrt{\frac{3SINR}{M-1}}\right) \quad (26)$$

Objective function:

$$\underset{\{\tau_k\}}{minimize}\, BER_{DHRR}(A_{DHRR}, \gamma, D_{DHRR}, H_{est}, N_S) \quad (27)$$

$$\text{Subject to: } c_1: trace\left(D_{DHRR} {D_{DHRR}}^H\right) \leq P_t$$
$$c_2: |\gamma_i|^2 = 1, \forall i, c_3 = |H - H_{est}| \leq \varepsilon$$

Where c_1 is power constraint at base station, c_2 is unit modulus constraint for RIS elements and c_3 is channel estimation constraint with ε being a permissible estimation error.

6. Data stream clustering EFCM

6.1 Algorithm design

Enhanced fuzzy C-means (EFCM) clustering emerges as an efficacious tool for partitioning data streams into public and private clusters, conducive to effective digital precoding. The algorithm judiciously classifies data into two coherent clusters, namely cluster A and B, leveraging a fuzzified membership function paired with a penalty term, and employs quantized symbols confined to the range, $[0, M-1]$ where M denotes the maximum value for symbol quantization. Given N_s Number of data streams, $N_{Samples}$ Number of samples per data stream and M maximum value for symbol quantization the function prototype is represented as follows:

$$F(N_s, N_{Samples}, M) \rightarrow (A, B, D) \quad (28)$$

Where A is the Indices of data streams belonging to cluster A, B is the Indices of data streams belonging to Cluster B, D is randomly generated quantized data streams and $F(.)$ represents the EFCM data clustering function.

6.2 Data generation and parameter initialization

Let D be a $N_S \times N_{Samples}$ matrix, where each element d_{ij} is an integer randomly selected from the discrete uniform distribution in the interval $[0, M-1]$. mathematically, this can be expressed as:

$$D = [d_{ij}] \quad (29)$$

Were,

$$0 \leq d_{ij} \leq (M-1), i = 1,2,..,N_S, j = 1,2,..,N_{samples}$$

This expresses that the data matrix D is populated with random integers in the specified range for each data stream and sample.

For EFCM, initial parameters are set as:

- $C = 2$: Number of clusters
- $m = 2$: Fuzzifier parameter to control the fuzziness of the membership matrix.
- max_{iter}=100: Maximum iteration limit
- $\epsilon = 10^{-5}$: Convergence tolerance

- $\vartheta = 0.5$: Penalty parameter.

6.3 Algorithm implementation

- ***Cluster initialization:*** Cluster centres V, and the membership matrix U, are initialized randomly. V is of dimension $C \times N_{Samples}$ and U is of dimension $N_S \times C$.
- ***Membership matrix update:*** The membership U_{ij} of the i^{th} data stream to cluster j is updated using:

$$U_{ij} = \frac{1}{\sum_{k=1}^{C}\left(\frac{\|data_i - V_j\|}{\|data_i - V_k\|}\right)^{\frac{2}{m-1}}} \tag{30}$$

- ***Cluster centres update:*** The penalty term ϑ, influences the update of the cluster centres V_j as follows:

$$V_j = \frac{\sum_{i=1}^{N_S}(U_{ij})^m . data_i}{\sum_{i=1}^{N_S}(U_{ij})^m + \vartheta\|V_j\|^2} \tag{31}$$

- ***Convergence check:*** If the difference between consecutive cluster centres is below the threshold ϵ, the algorithm converges.
- ***Cluster assignment:*** The data streams are assigned to clusters A and B, based on the highest membership value in U.

6.4 Integration with digital precoder

Following the classification of data streams into either cluster A or B through EFCM, this classified data is subsequently fed into a digital precoder over varying time scales. Utilizing both public and private data streams facilitates the development of a robust digital precoding strategy, thereby enhancing communication system performance by optimizing signal quality and reducing interference. This modular approach introduces an innovative pathway to explore novel data stream clustering methodologies, inviting future works to explore diverse clustering algorithms in digital precoding applications. Further explorations may navigate through optimizing parameter tuning and exploring the applicability in various communication models.

7. Channel estimation in MIMO systems using ABPNN for DHRR RIS-assisted communications

In the proposed DHRR-RIS system, ensuring precise CSI estimation is crucial for both the channels: from the BS to the DHRR RIS, and from the DHRR RIS to UT. The ABPNN emerges as an effective solution for this dual-channel estimation. For an ABPNN algorithm used for channel estimation, we focused on minimizing MSE with increasing epochs.

$$MSE = \frac{1}{g}\sum_{I=1}^{g}(\hat{h}_i - h_i)^2 \tag{32}$$

Where g number of samples in the dataset, $\hat{h}_i$ is the estimated Channel response by ABPNN and h_i is the true channel response. The BS transmits the pilot sequence, represented by Eq. (33), and for downlink, the Eq. (34) depicts the pilot sequence sent by the US.

$$X_{BS-DHRR} = A_{DHRR}{S_{pilot}}^{BS} \tag{33}$$

$$X_{DHRR-UT} = W_{DHRR}{S_{pilot}}^{UT} \tag{34}$$

Where $X_{BS-DHRR}$ and $X_{DHRR-US}$ are the pilot sequences, A_{DHRR} is the Analog Precoder matrix and W_{DHRR} is the analog combiner matrix. ${S_{pilot}}^{BS}$ and ${S_{pilot}}^{UT}$ are the transmitted symbol sequences of Base Station and User terminal respectively.The ABPNN architecture comprises three pivotal layers: input as shown in Eq. (35), hidden shown in Eq. (36), and output shown in Eq. (37).

$$\mathrm{X} = (\mathrm{X}_1, \mathrm{X}_2, \ldots, \mathrm{X}_\mathrm{n})^\mathrm{T} \tag{35}$$

$$\mathrm{hid_i} = \mathrm{act}_1\left(\sum_{\mathrm{j}=1}^{\mathrm{n}} \mathrm{we_{ij}X_j} - \mathrm{Th_i}\right) \tag{36}$$

$$\mathrm{op_i} = \mathrm{act}_2\left(\sum_{\mathrm{j}=1}^{\mathrm{m}} \mathrm{cwe_{th,j}\ hid_i} - \mathrm{cwe_{th}}\right) \tag{37}$$

$$\widehat{\mathrm{op}}_{\mathrm{forecast}} = (\widehat{\mathrm{op}}_\mathrm{i} + 1)\big(\mathrm{maxi(op_i)} - \mathrm{mini(op_i)} + \mathrm{mini(op_i)}\big) \tag{38}$$

$$\mathrm{Err} = \frac{1}{2}\sum_{l}^{\mathrm{L}}(\mathrm{op_l} - ex\mathrm{op_l})^2 \tag{39}$$

$$\vartheta_\mathrm{l} = (ex\mathrm{op_l} - \mathrm{op_l})\mathrm{op_l}(1 - \mathrm{op_l}) \tag{40}$$

$$\mathrm{errc_j} = \left(\sum_{l}^{\mathrm{L}} \mathrm{cwe_{th,j}} * \mathrm{Err}\right)\mathrm{hid_i}\ (1 - \mathrm{hid_i}) \tag{41}$$

$$CV = bwd(fwd(CV; \Xi_e); \Xi_{rt}) \tag{42}$$

$$H_{est} = (Q[\mathrm{CV}]) \tag{43}$$

The network iteratively refines its weights, aiming to minimize the error between the estimated and actual channel responses. The estimated channel vectors are then relayed to the transmitters and receivers. Following this, feedback in terms of the

achievable rate is obtained and channelled back to the RIS.

The subsequent phase involves reconstructing the channel vector, as shown in Eq. (43), and its quantization to achieve a robust hybrid precoder design. This approach not only ensures accurate channel estimation but also caters to the dynamically changing wireless environment, making ABPNN a cornerstone for the proposed DHRR-RIS system.

8. Hybrid precoder and combiner design using DDPG

The DDPG algorithm, an adaptation of deep Q-learning to the continuous action domain, is instrumental in optimizing the digital (D_{DHRR}) and analog (A_{DHRR}) precoders in a massive MIMO communication system. The state $S(t)$ representing the system at time t is characterized by the channel state information (CSI), $H(t)$, and the current precoder matrices. The action $A(t)$ is defined as the adjustment applied to the precoder matrices. The reward function $R(t)$ is crafted as a composite metric involving the SNR and the BER as:

$$R(t) = w_1.SNR(t) - w_2.BER(t) \tag{44}$$

Subject to $c_1: \|F\|_D^2 \leq P_t$,
$c_2: \gamma_i \in (0,2\pi), 0 \leq \gamma_i \leq 2\pi$

where w_1 and w_2 are the weighting factors indicating the trade-off between SNR and BER. Employing the DDPG algorithm begins with initializing the actor and critic networks and their corresponding target networks. The exploration-exploitation strategy, such as the Ornstein-Uhlenbeck process, is adopted to explore the action space proficiently.

Critic update: Utilizing sampled experiences (S, A, R, S') from the replay buffer, the critic network is updated by minimizing the mean squared error (MSE) loss between the predicted Q-value and the target Q-value, which is computed as:

$$Q_{target}(t) = R(t) + \delta Q'\left(,\mu'\big(S'(t)\big)\right) \tag{45}$$

$$Loss_C = MSE\big[Q\big(S(t), A(t)\big), Q_{target}(t)\big] \tag{46}$$

Where Q' and μ' represent the critic and actor target networks and δ is the discount factor.

Actor update: The actor network is refined by maximizing the expected cumulative reward, which is approximated using the gradient of the critic network with respect to the action, expressed as:

$$\nabla_{\theta_\mu} J \approx \frac{1}{N}\sum_{i=1}^{N} \nabla_a Q(S, A|\phi)_{S=S_i, A=\mu(S_i)} \nabla_{\theta_\mu}(S|\,\theta_\mu)_{S_i} \tag{47}$$

Where N is the batch size, and θ_μ and ϕdenotes the actor and critic networks respectively.

Soft target updates: The target networks are softly updated using,

$$\theta_\mu{}' \leftarrow \tau\theta_\mu + (1-\tau)\theta_\mu{}' \tag{48}$$

$$\phi' \leftarrow \tau\phi + (1-\tau)\phi' \tag{49}$$

Where $0 < \tau \ll 1$ ensures slow tracking of the learned networks.

Output precoders: The optimized actor network provides the policy for selecting actions, thus providing the optimized precoders, expressed as:

$$D_{DHRR}(t) = \mu_{D_{DHRR}}\big(S(t)\big|\theta_\mu\big) \tag{50}$$

$$A_{DHRR}(t) = \mu_{A_{DHRR}}\big(S(t)\big|\theta_\mu\big) \tag{51}$$

By iteratively updating the actor and critic networks, the DDPG algorithm yields optimized digital precoder matrix $D_{DHRR}(t)$ and $A_{DHRR}(t)$, enhancing communication performance by adaptively shaping the transmitted signals to navigate through the wireless channel optimally. In a symmetrical vein, the digital and analog combiners, Wd_{DHRR} and Wa_{DHRR} respectively, at the receiver end are optimized using a similar approach. The combiner design's objective is primarily to maximize the received signal to noise ratio (SNR) while mitigating interference and preserving the integrity of the transmitted signal amidst the wireless channel's impairments.

Given the state $S'(t)$, comprised of the received signal matrix and the current combiners' status, the DDPG algorithm endeavors to learn a policy that iteratively updates the combiners to enhance the received signal quality. The action $A'(t)$ herein is typified as the incremental adjustment to the combiner matrices. Defining the reward function as $R'(t) = w_3.SNR'(t) - w_4.BER'(t)$ arbitrate the emphasis between SNR and BER in the reward landscape, the adaptation of the combiner matrices unfolds.

Critic update: Analogous to the precoder design, the critic network updates leverage sampled experiences.

(S', A', R', S'') from the replay buffer and minimize the MSE loss between predicted and target Q-values, mathematically represented as:

Table 2. Parameters for proposed DDPG in designing hybrid precoder

Parameter	Description
State $S(t)$	The clustered N_S and H_{est} between BS and DHRR RIS at the current time stamp
Action $A(t)$	Performs optimization of DAC-RF Chain pairs
Reward $R(t)$	minimize MSE and maximize achievable rate

$$Q'_{target}(t) = R'(t) + \delta Q''\left(,\mu''\left(S''(t)\right)\right) \quad (52)$$

$$Loss_{C'} = MSE\left[Q'\left(S'(t), A'(t)\right), Q'_{target}(t)\right] \quad (53)$$

Actor update: The actor network, conversely, optimizes for the cumulative expected reward. The update is accomplished by considering the gradient from the critic network with respect to the action, expressed as:

$$\nabla_{\theta_{\mu'}} J \approx \frac{1}{N'}\sum_{i=1}^{N'} \nabla_a Q(S', A'|\phi')_{S'=S'_i, A'=\mu'(S_i')} \nabla_{\theta_{\mu'}}(S'|\theta_{\mu'})_{S_i'} \quad (54)$$

Soft target updates: Similar soft updates are performed for the target networks as follows:

$$\theta_{\mu'}' \leftarrow \tau'\theta_{\mu'} + (1-\tau')\theta_{\mu'}'' \quad (55)$$

$$\phi'' \leftarrow \tau'\phi' + (1-\tau')\phi'' \quad (56)$$

Where τ' is a small positive factor ensuring slow tracking of the learned networks.

In both analog and digital combiner cases, the outputs are given by:

$$Wd_{DHRR}(t) = \mu_{Wd_{DHRR}}\left(S'(t)\middle|\theta_{\mu'}\right) \quad (57)$$

$$Wa_{DHRR}(t) = \mu_{Wa_{DHRR}}\left(S'(t)\middle|\theta_{\mu'}\right) \quad (58)$$

The convergence towards optimal combiners, Wd_{DHRR} and Wa_{DHRR} is facilitated by iteratively applying the DDPG updates, thereby navigating through the action space to uncover combiner matrices that uphold the integrity and reliability of the received signals in a massive MIMO context.

9. DHRR RIS design using FHO algorithm

In leveraging the FHO algorithm for optimizing the DHRR-RIS in a MIMO system, the integration of appropriate constraints and a well-defined cost function is crucial.

Table 3. Parameters for proposed DDPG in designing hybrid combiner

Parameter	Description
State $S(t)$	The received signal at the DHRR RIS, noise levels and the H_{est} between DHRR RIS and UT at the current time stamp.
Action $A(t)$	Optimization of combining weights to minimize interference and maximize signal quality for the desired signal.
Reward $R(t)$	A function that rewards minimizing the BER and maximizing the Signal to Noise Ratio (SINR) at the receiver.

$$cost = -SNR = -\frac{|h_{eff}w|^2}{\sigma^2} \quad (59)$$

Where h_{eff} is the effective channel including the DHRR RIS, w is the beamforming vector and σ^2 is the noise power. This optimization process revolves around minimizing the cost so negative SNR.

Hawk position representation: The position of each hawk in the FHO algorithm, $X^{(k)}$, corresponds to a potential RIS configuration. For passive elements, it represents phase shifts, and for active elements, both amplification factors and phase shifts:

$$X^{(k)} = \begin{cases} |\tau_k| e^{j\emptyset_k}, & if\ k \in B \\ e^{j\emptyset_k}, & otherwise \end{cases} \quad (60)$$

where τ_k and $e^{j\theta_k}$ denote the amplitude and phase shift introduced by the RIS element i respectively and $B \subseteq \{1,2,\ldots,M\}$ which is a set of position of L active elements.

FHO iterative position update: The new position of the i^{th} hawk ${X_{new}}^{(k)}$, is updated based on its old position ${X_{old}}^{(k)}$, and the positions of the best-performing hawk, ${X_{best}}^{(k)}$, influenced by constants $\varkappa$ (exploitation) and ϱ (exploration), along with a random complex number $\xi^{(k)}$ to introduce randomness as shown below:

$${X_{new}}^{(k)} = {X_{old}}^{(k)} + \varkappa \times \left({X_{best}}^{(k)} - {X_{old}}^{(k)}\right) + \varrho \times \xi^{(k)} \quad (61)$$

Phase shift matrix for passive elements: To pragmatically integrate the FHO within the DHRR-RIS system, the passive elements introduce a phase shift to the incident signal, while active elements impart amplification alongside phase modulation.

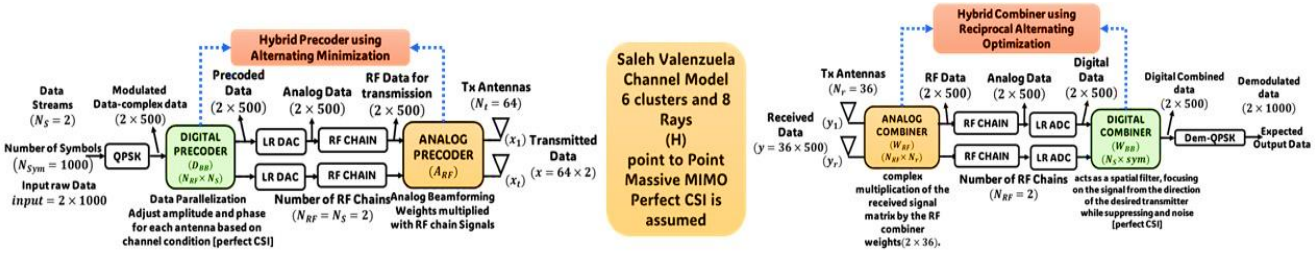

Figure. 4 Simulation model of first approach

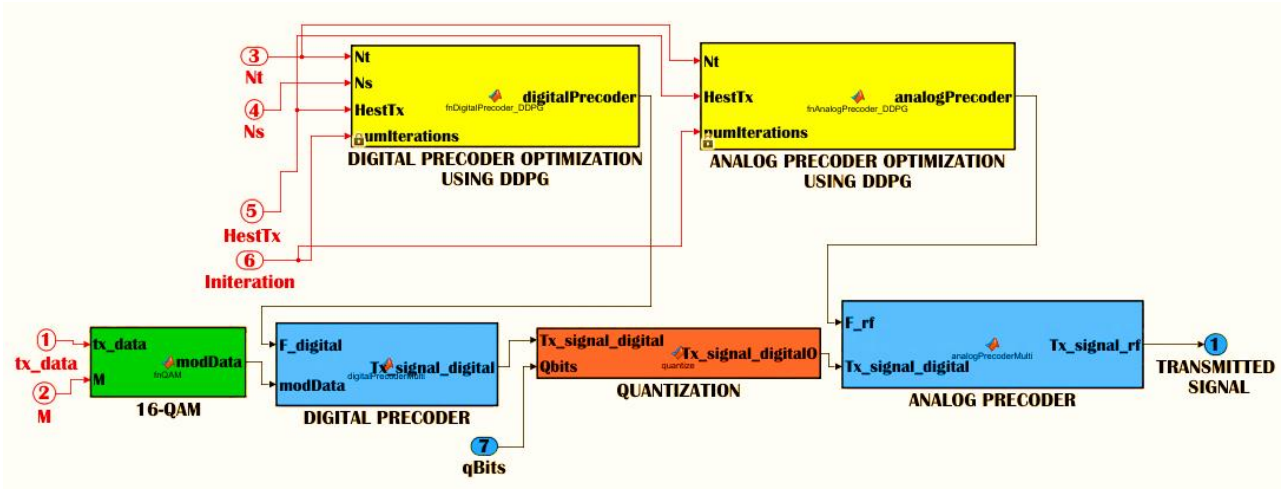

Figure. 5 Base station simulink model of DHRR RIS based hybrid precoder for massive MIMO

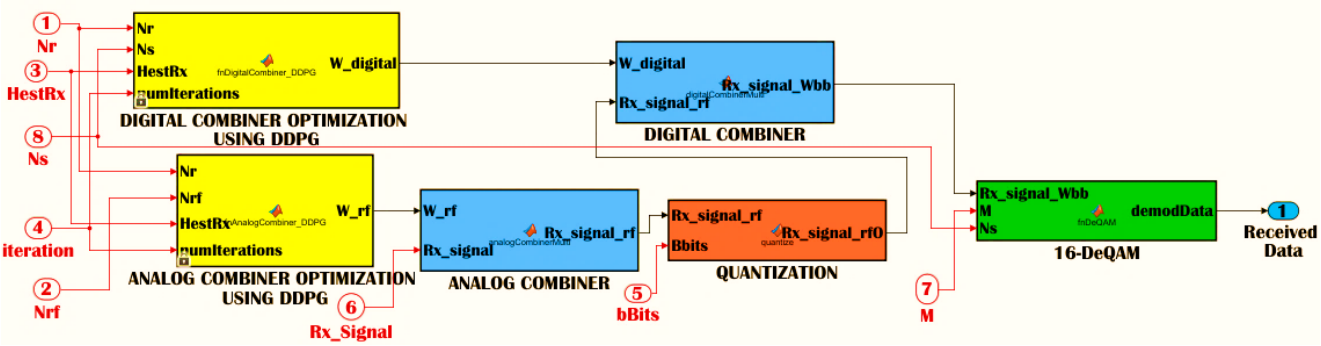

Figure. 6 User terminal simulink model of DHRR RIS based hybrid precoder for massive MIMO

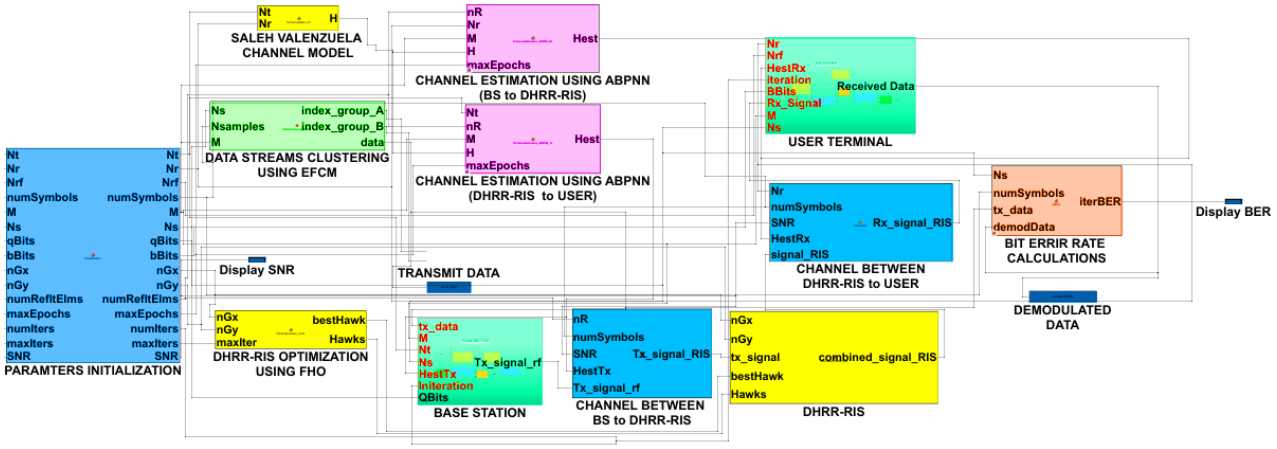

Figure. 7 Overall simulink model of DHRR RIS based hybrid precoder for massive MIMO

The phase shift introduced by the passive elements, being a function of their position in the search space X, can be represented by a phase shift matrix P:

$$P = diag\left(e^{j\emptyset_1}, e^{j\emptyset_2}, \dots\dots\dots, e^{j\emptyset_V}\right) \quad (62)$$

where V is the number of passive elements, and each $e^{j\theta_V}$ denotes the complex exponential representing the phase shift introduced by the i^{th} passive element.

Amplification matrix for active elements: The active elements L in number, involve an amplification factor $|\tau_k|$ alongside the phase modulation, formulated as an amplification matrix G which is formulated as:

$$G = diag\left(|\tau_1|e^{j\emptyset_1}, |\tau_1|e^{j\emptyset_2}, \dots\dots\dots, |\tau_L|e^{j\emptyset_L}\right) \quad (63)$$

Where with $|\tau_k|$ and $e^{j\emptyset_L}$ as the amplification factor and phase introduced by the i^{th} active element.

10. Simulation results

This paper presents two distinct studies on massive MIMO systems, each exploring different facets and yielding insightful findings. The first study focuses on a single-user MIMO system, where the key strategy was implementing NniQ in low-resolution DACs and ADCs, challenging the norm of UniQ. The second study extended the scope to multi-user MIMO systems, introducing RIS and machine learning algorithms. Unlike the first study, this approach harnessed the power of machine learning algorithms for various tasks.

We implemented MATLAB simulation for our first approach as shown in Fig. 4 and simulink model for our second approach as shown in Figs. 5-7 using MATLAB R2023a tool, think station Lenovo computer with 256GB RAM and AMD Rygen Threadripper PRO 32 cores processor and compared it with existing works using several validation metrics. Our results show that our first approach yields a very good result for NniQ as compared to UniQ low resolution ADCs/DACs are considered and our second approach outperforms existing works in terms of WSR, and BER.

10.1 Comparative analysis of NniQ and UniQ massive MIMO system

The first study meticulously evaluates the SE of a hybrid precoder setup, integrating advanced DACs and ADCs within a base station featuring N_t transmitting antennas addressing a single-user with a 36-antenna receiver setup. Our exploration is dual-focused, encompassing UniQ and NniQ.

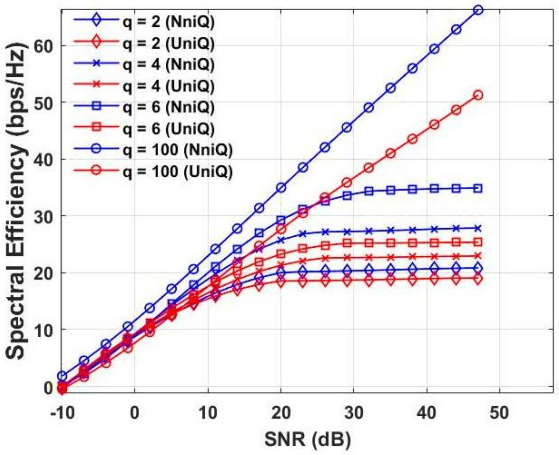

Figure. 8 SE vs SNR with $q = 2,4,6,100\ bits$ and $b = 100\ bits$

Table 4 SE (bps/Hz)- Varying q

Type	DAC Resolution (q)		
	2 *bits*	**4 *bits***	**6 *bits***
NniQ	19.79	26.44	31.53
UniQ [3]	18.77	21.51	24.97
Data Rate (*Gbps*)	NniQ-3.9 UniQ-3.7	NniQ-5.2 UniQ-4.3	NniQ-6.3 UniQ-4.9
Improved	5.43%	22.91%	26.27%

In our detailed assessment as shown in Fig. 4, we examined the Hybrid Precoded Massive MIMO system's performance with $N_t = 64$, $N_r = 36$, $N_s = 2$ and $N_{RF}{}^t = 2$ underscoring the influence of varied ADC and DAC resolutions with both b and q equal to $2,4,6\ bits$ under diverse quantization and SNR scenarios.

Fig. 8 emphasizes varied q which indicates SE performances between UniQ and NniQ beyond an SNR of $-10dB$. This efficiency surges with increased q and b, with NniQ outperforming UniQ in high-resolution scenarios.

NniQ's bit economy is evident, showcasing pronounced SE at higher SNRs. At lower SNRs, UniQ and NniQ perform similarly due to close Gaussian white noise and transmitted power levels. Crucially, NniQ is notably superior in low-resolution DAC setups, highlighting its suitability for efficient, high-quality transmissions in Massive MIMO systems. Fig. 9, emphasizing varied b, reveals that elevating ADC resolution significantly boosts SE, eventually mirroring a system without quantization distortions. This hints at an optimal threshold for

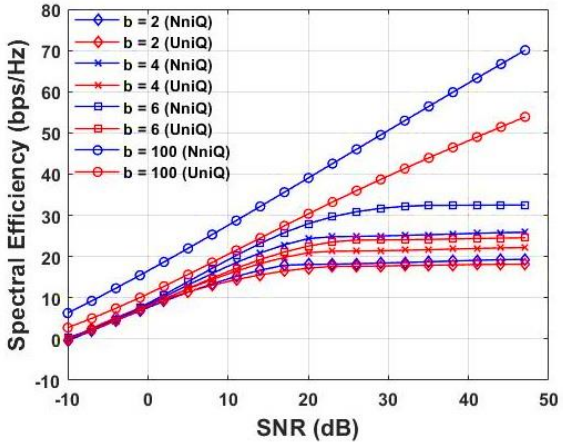

Figure. 9. SE vs SNR wit $b = 2,4,6\ bits$ and $q = 100\ bits$

Table 5 SE (bps/Hz) for Varying b

Type	**ADC Resolution (b)**		
	2 *bits*	**4 *bits***	**6 *bits***
NniQ	22.35	28.56	33.74
UniQ [3]	21.26	23.7	26.54
Data Rate (*Gbps*)	NniQ-4.4 UniQ-4.2	NniQ -5.7 UniQ -4.7	NniQ -6.7 UniQ -5.3
Improved	5.12%	20.50%	27.12%

resolution enhancement.

Theoretically, NniQ's adaptability to allocate quantization levels based on signal amplitude distributions sets it apart. This approach, in contrast to UQ's linear strategy, optimally manages quantization levels, especially in varying wireless signal environments. As a result, NniQ maintains a BER and ensures enhanced link stability.

However, the simulation results emphasizes that low resolution DAC and ADC benefits with enhanced SE and NniQ works much better than UniQ in both the scenarios as shown in Tables 4 and 5. This is attributed to NniQ's adept quantization mechanism, minimizing noise, and optimizing power use, unlike UniQ's more rigid method.

Figs. 10 and 11 delve into the EE-SE relationship trade-off curve concerning q and b. Collectively, they highlight NniQ's advantage in achieving superior EE, particularly at reduced SNRs.

In Tables 6 and 7, we present a comparative analysis of power consumption for the system under study, contrasting the results between UniQ and NniQ with a fully digital precoding approach.

The fully digital precoding method, where each antenna is connected to individual RF chains,

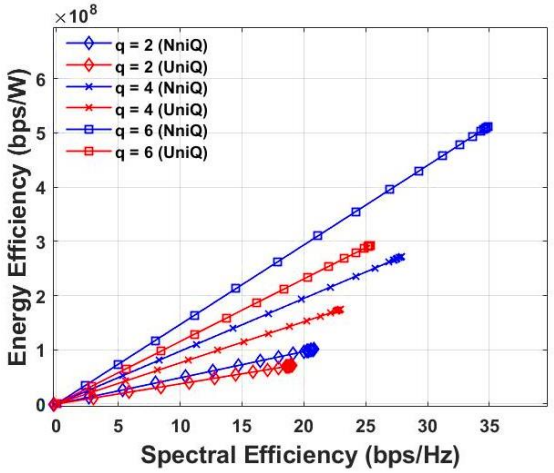

Figure.10 EE vs. SE comparison for varied q with $b = 6\ bits, SNR = -5dB$

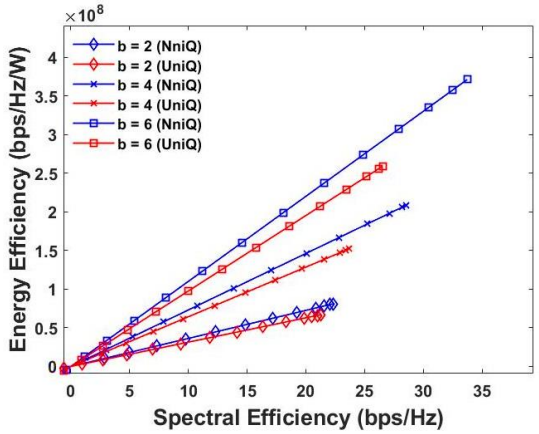

Figure. 11 EE vs. SE comparison for varied b with $q = 3\ bits, SNR = -5dB$

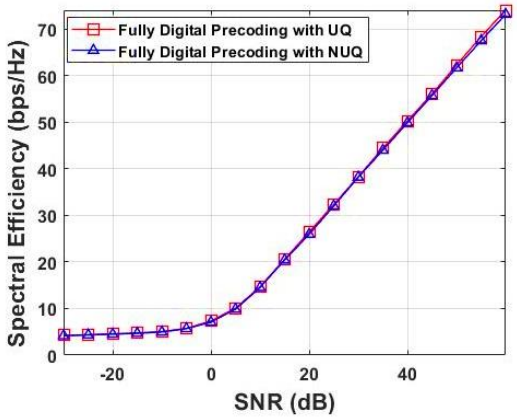

Figure. 12. SE vs SNR for fully digital precoding

achieves a spectral efficiency of 70bps/Hz as shown in Fig. 12 while consumes 94 watts of power.

In contrast, the NniQ approach attains a comparable data rate but demonstrates a significant reduction in power consumption, requiring only 6 watts. This reduction, however, comes with a trade-off in spectral efficiency, where NniQ delivers 35bps/Hz.

Table 6. Power consumption and data rate varying q with $b = 6bits$

Performance Metrics	**NniQ**	**UniQ**
	$\boldsymbol{q = 2\ bits}$	
EE $(\boldsymbol{Gbps/W})$	0.096	0.068
Power Consumed $(\boldsymbol{mW})$	6166.37	6851.53
Data rate	$591Mbps$	$465Mbps$
	$\boldsymbol{q = 4\ bits}$	
EE $(\boldsymbol{Gbps/W})$	0.257	0.185
Power Consumed $(\boldsymbol{mW})$	6166.41	6851.57
Data rate	$1.58Gbps$	$1.26Gbps$
	$\boldsymbol{q = 6\ bits}$	
EE $(\boldsymbol{Gbps/W})$	0.462	0.32
Power Consumed $(\boldsymbol{mW})$	6166.44	6851.60
Data rate	$2.84Gbps$	$2.19Gbps$

Table 7. Power consumption and data rate varying b with $q = 3bits$

Performance Metrics	**NniQ**	**UniQ**
	$\boldsymbol{b = 2\ bits}$	
EE $(\boldsymbol{Gbps/W})$	0.080	0.066
Power Consumed	6165.54	6850.61
Data rate	$493Mbps$	$452Mbps$
	$\boldsymbol{b = 4\ bits}$	
EE $(\boldsymbol{Gbps/W})$	0.214	0.157
Power Consumed	6165.72	6850.80
Data rate	$1.31Gbps$	$1.07Gbps$
	$\boldsymbol{b = 6\ bits}$	
EE $(\boldsymbol{Gbps/W})$	0.371	0.258
Power Consumed	6166.39	6851.55
Data rate	$2.28Gbps$	$1.76Gbps$

This comparison underscores the energy efficiency of NniQ in achieving substantial power savings at the cost of reduced spectral efficiency, a crucial consideration for the design of massive MIMO systems.

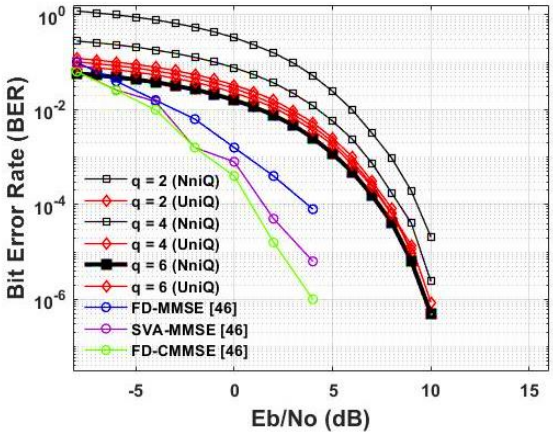

Figure.13 BER vs Eb/N0 for NniQ and UniQ when DAC resolution of 2,4 and 6 bits considered

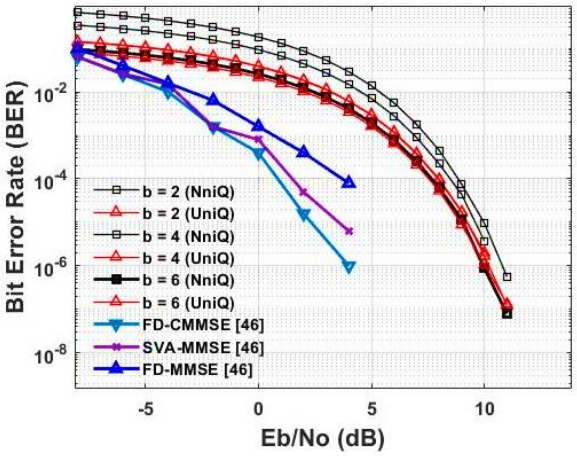

Figure. 14 BER vs Eb/N0 for NniQ and UQ when ADC resolution of 2,4 and 6 bits considered

Table 10. BER vs E_b/N_O - varying DAC resolution at base station

Type	**DAC Resolution** $(\boldsymbol{q})$		
	2 $\boldsymbol{bits}$	**4** $\boldsymbol{bits}$	**6** $\boldsymbol{bits}$
NniQ	2.07×10^{-7}	1.17×10^{-6}	7.14×10^{-7}
UniQ	2.63×10^{-7}	3.60×10^{-7}	8.34×10^{-8}
FD CMMSE [46]	1.12×10^{-6}		
SVA MMSE [46]	6.31×10^{-6}		
FD MMSE [46]	7.94×10^{-5}		

Employing quadrature phase shift keying (QPSK) modulation, known for its balance between data rate and reliability, the system under NniQ and UniQ conditions exhibits notable robustness compared with different MMSE techniques shown in [46].

Table 11. BER vs E_b/N_O - Varying DAC resolution at base station

Type	ADC Resolution (b)		
	2 *bits*	**4 *bits***	**6 *bits***
NniQ	3.74×10^{-6}	5.64×10^{-7}	7.99×10^{-8}
UniQ	2.01×10^{-6}	1.21×10^{-7}	1.34×10^{-7}
FD CMMSE [46]	1.12×10^{-6}		
SVA MMSE [46]	6.31×10^{-6}		
FD MMSE [46]	7.94×10^{-5}		

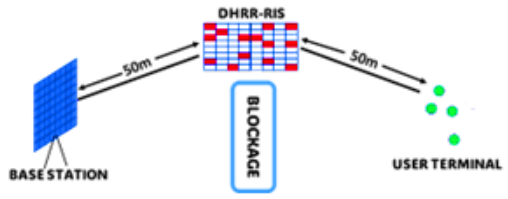

Figure. 15 Simulation model of second approach

The graph as shown in Figs. 13 and 14, presents the BER for a massive MIMO system employing hybrid precoders and combiners designed via alternating minimization and reciprocal alternating optimization algorithms, respectively. It evaluates the system performance over a range of E_b/N_0 values for different DAC/ADCs resolutions under two quantization schemes: UniQ and NniQ.

Lower BER is achieved with NniQ across all DAC/ADCs resolutions as shown in Tables 10 and 11, highlighting its efficiency in handling signal details. The BER curves for the UniQ and NniQ converge toward those of the benchmark techniques (FD-MMSE, SVA-MMSE, FD-CMMSE) as Eb/No increases, indicating that despite the lower resolution DACs, the system approaches the performance of more traditional MIMO systems at higher signal-to-noise ratios.

10.2 Optimization and efficacy of hybrid precoder design in leveraging machine learning and reconfigurable intelligent surfaces

This work examines the efficacy of a hybrid precoder and combiner design using 64 M_{BS} transmitter antennas with half wavelength spacing and 4 users with each user 4 (M_{UT}) user antennas distributed among UT users as shown in Fig. 15, at a carrier frequency of 28 GHz and bandwidth of 200MHz.

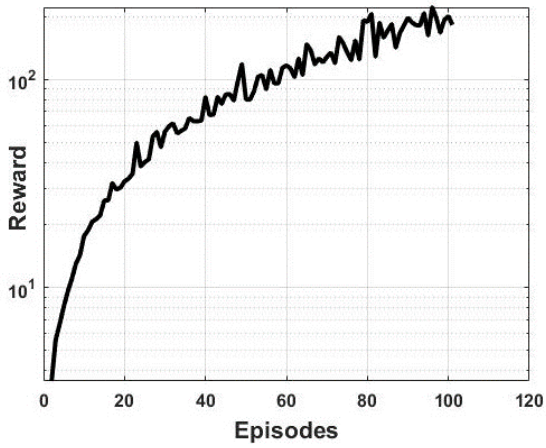

Figure. 16 reward vs episodes

The simulations utilized 1,000 symbols and employed 4-bit DACs and ADCs with 16 QAM modulation scheme. These symbols are clustered into private and public streams using EFCM algorithm.

The hybrid precoder and combiner were designed using a DDPG algorithm, while channel estimation was performed with ABPNN algorithm. Additionally, DHRR-RIS were designed using the fire hawk optimization technique.

Over 500 iterations, the system's performance and reliability were analysed using monte carlo simulations, with ensuing sections providing a detailed examination of the obtained data, revealing insights into the system's behaviour and performance under the stipulated configurations.

10.2.1. Simulation outcomes of machine learning algorithms

10.2.1.1. DDPG for hybrid precoder optimization

The DDPG algorithm was configured with distinct learning rates for the critic (0.001) and actor (0.0001) networks, optimizing the balance between stability and convergence speed. A carefully managed noise variance decay strategy ensured an effective balance between exploration and exploitation throughout the training process.

The algorithm's ability to address the high dimensionality and computational constraints in massive MIMO systems showcases its robustness. By leveraging a large experience buffer and an appropriate discount factor, DDPG facilitated an efficient design process, tailoring the precoder and combiner weights to achieve optimal performance as shown in Fig. 16 and Table 12 within the constraints of real-time processing demands.

10.2.1.2. ABPNN for channel estimation optimization

The ABPNN algorithm demonstrated

Table 12. DDPG parameter settings and simulation results

Parameter	Value
Configurations	
Critic Network Learning Rate	0.001
Critic Gradient Threshold	1
Actor Network Learning Rate	0.0001
Actor Gradient Threshold	1
Target Smooth Factor	0.001
Experience Buffer	1×10^6 *steps*
Discount Factor	0.99
Minibatch Size	32
Noise Variance	0.3 *to* 10^{-6}
Simulation Outcomes	
Max Episodes	100
Max Steps Per Episode	20
Training Stop Criterion	Average Reward -66
Computational Time	*1991 seconds*

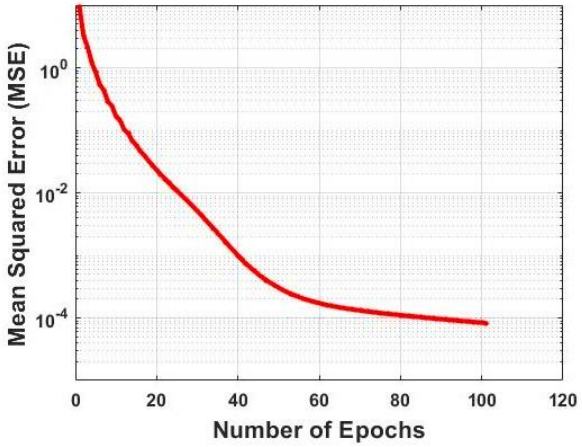

Figure. 17 MSE vs maximum epochs

considerable efficacy in channel estimation between the BS and DHRR-RIS, and from DHRR-RIS to the UT. Employing a dual-layer structure with 100 and 2304 nodes respectively, the ABPNN was optimized using a scaled conjugate gradient training algorithm. An initial learning rate of 0.01, adjusted by increase and decrease factors of 1.05 and 0.7, underpinned the network's adaptive learning capability.

The learning process was characterized by a notable reduction in MSE, reaching a final training MSE of 8.6706×10^{-5}, with validation and test MSEs converging around 8.99×10^{-4}. The ABPNN's adaptation culminated after 100 epochs as shown in Fig. 17 and Table 13, with the entire process executed in 1978.43 seconds.

This approach highlights the ABPNN's robustness in capturing the complex characteristics of the wireless channel, enhancing the accuracy of channel state information and potentially contributing to the optimization of signal transmission in advanced communication systems.

Table 13. ABPNN configuration and performance outcomes

Parameter	Value
Configurations	
Hidden Layers	[100, 2304]
Training Algorithm	Scaled Conjugate
Initial Learning Rate	0.01
Increase Factor	1.05
Decrease Factor	0.7
Simulation Outcomes	
Final Training MSE	8.6706×10^{-5}
Final Validation MSE	8.994276×10^{-4}
Final Test MSE	8.6795×10^{-4}
Total Epochs	100
Computational Time	1978.43 seconds

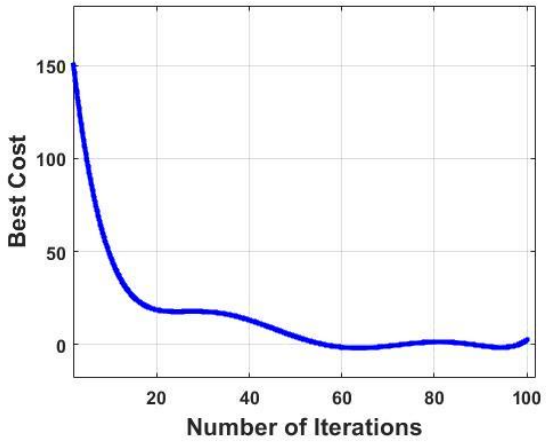

Figure. 18 Best cost vs maximum iterations

10.2.1.3. FHO for DHRR RIS optimization

The fire hawk optimization (FHO) algorithm was employed for the strategic design and optimization of a dynamic hybrid relay reconfigurable intelligent surface (DHRR-RIS).

This novel optimization method was applied to a RIS configuration consisting of 64 elements, with 8 active and 56 passive elements.

The graphical representation of the optimization process, as shown in Fig. 18, demonstrates a rapid decrease in cost as the number of iterations increases.

Table 14. FHO design specifications and optimization achievements

Parameter	Value
Configurations	
RIS Configuration	64 elements (8 active, 56 passive)
Simulation Outcomes	
Best Cost	0.00099114
Iterations	100
Total Evaluations	11,608
Computational	1160.8seconds

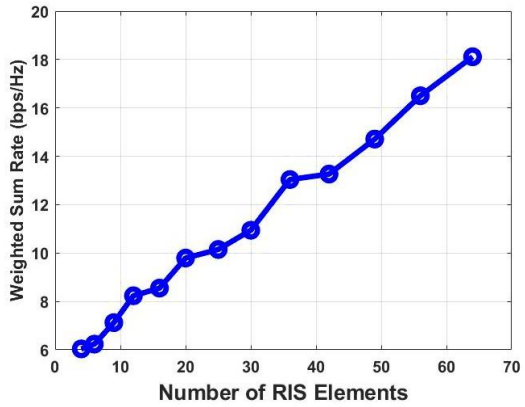

Figure. 19 WSR vs reflecting elements of DHRR RIS (Proposed Work)

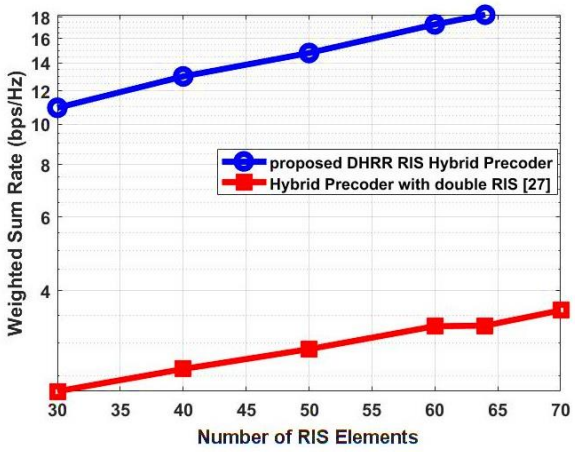

Figure. 20 WSR vs number of RIS elements (comparative analysis)

After 100 iterations, the FHO algorithm achieved an optimal cost of 0.00099114. The process involved a total of 11,608 evaluations, reflecting the algorithm's thorough search for an optimal solution within the design space as shown in Table 14.

Although the computational time was not specified, the trajectory of the cost curve suggests a swift convergence, indicative of the FHO algorithm's efficiency.

This optimization contributes to the RIS's ability to dynamically adapt to varying channel conditions, potentially enhancing the performance of wireless communication networks.

10.3 WSR analysis

10.3.1. Comparative analysis of WSR performance with increasing DHRR-RIS elements

In our proposed DHRR RIS, we harness the FHO algorithm to strategically select superior reflecting elements in DHRR RIS, pivotal for efficient analog beamforming. Proper calibration of these elements is crucial, directly influencing the WSR, a primary indicator of system performance.

Our analysis, detailed in Fig. 19, indicates a direct relationship between the WSR and the array of reflecting elements. A higher count of these elements correlates with improved WSR. This method stands out compared to prior works as shown in Fig. 20, primarily due to the optimization techniques applied to configure reflecting elements in intelligent surfaces.

Our approach involves using a DHRR-RIS to facilitate sophisticated analog beamforming, essential for effective hybrid precoding. We employ the FHO algorithm to optimize the arrangement of phase shifters in passive elements.

This optimization of reflecting elements within the DHRR-RIS leads to a maximized WSR, an enhancement over existing methods. Additionally, while the DRIS-HP [27] method uses the reflective modulation optimization (RMO) algorithm for phase shift fine-tuning, it faces challenges due to its high computational demands, further impacting the WSR negatively. Our proposed work as achieved 18bps/Hz by considering 64 DHRR RIS elements whereas the DRIS-HP has achieved approximately 3.9bps/Hz by

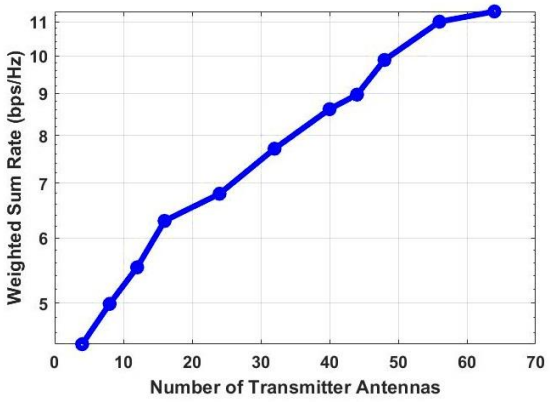

Figure. 21 WSR vs varying antennas at base station (proposed work)

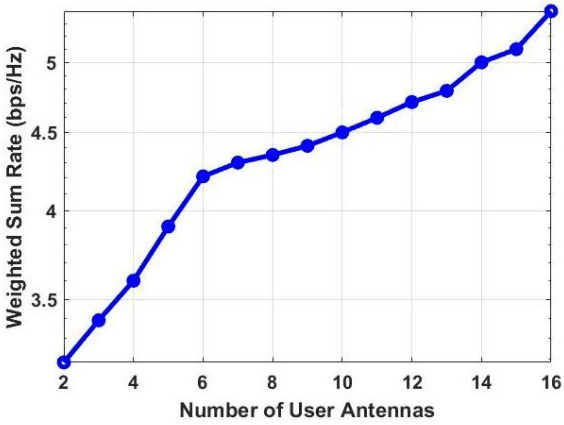

Figure. 22 WSR vs varying user antennas (proposed work)

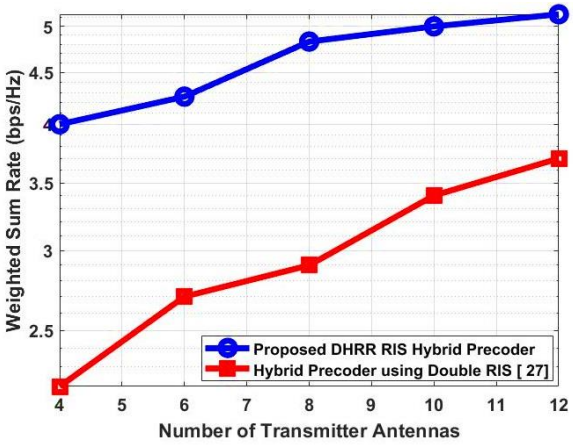

Figure. 23 WSR vs varying antennas at base station (comparative analysis)

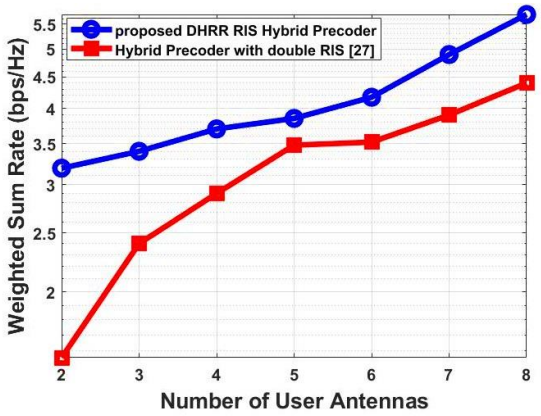

Figure. 24 WSR vs varying user antennas (comparative analysis)

considering dual RIS with 100 reflecting elements.

10.3.2. Comparative analysis of WSR performance with varying transmitter and receiver antennas

In the proposed communications framework, the roles of transmitter and receiver antennas, integral to base stations and user terminals, are critical. Their optimization and balanced operation are essential for effective communication within the network.

Figs. 21 and 22 depict the analysis of WSR relative to the intricate configurations of the transmitter and receiver antennas whereas Figs. 23 and 24 depict the comparative analysis with the existing work.The data indicates that the proposed method achieves an enhanced WSR compared to existing strategies. This improvement stems from an innovative approach to antenna optimization, which involves considering minimum number of connected RF chains and Low-resolution DAC/ADC pairs.

This approach minimizes unnecessary energy consumption and operational complexity during transmission phases, leading to a noticeable increase in WSR.

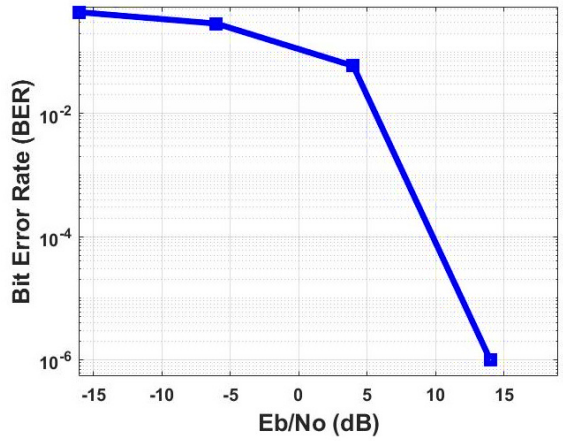

Figure. 25 BER vs SNR (proposed work)

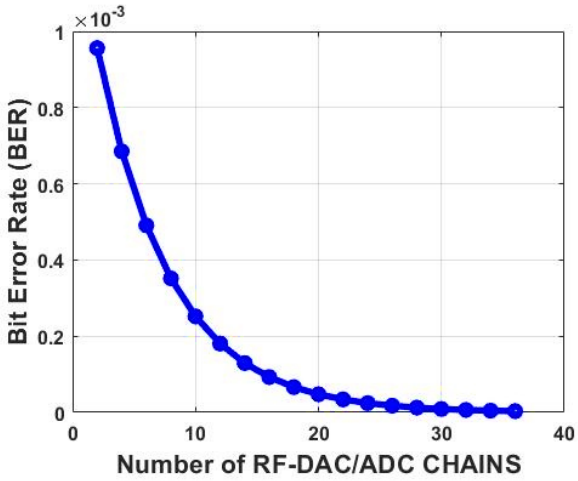

Figure. 26 BER vs varying RF-DAC/ADC chains (proposed work)

In contrast, existing models like DRIS-HP [27] incorporate advanced deep learning techniques for hybrid precoding design but fall short in addressing inefficiencies and complexities in antenna functions, resulting in a lower WSR.

Subsequent analysis reveals similar trends with receiver antennas; an increase to 8 antennas sees our WSR rise to 5.7 bps/Hz, a marked improvement over the 4.4 bps/Hz achieved by DRIS-HP.

Our simulation results further highlight this efficiency: when the transmitter antennas are increased to 12, our system's WSR peaks at 5.14 bps/Hz, outperforming DRIS-HP which register 3.7 bps/Hz. The observed differential in performance underscores the efficacy of our proposed system.

10.3.2.1. Comparative analysis of BER performance with varying SNR and RF-DAC/ADC chains

An initial examination of the BER in relation to the signal to noise ratio (SNR) disclosed a notable reduction in BER from 10^{-1} to 10^{-6} as the SNR intensified, this is clearly depicted in Fig. 25.

Established theory suggests a high SNR, given the system's optimal operation and perfect channel states, is expected to correspond to a lowered BER. This principle was conspicuously confirmed by the simulation data, where the $BER - SNR$ graph demonstrated consistent enhancements in error rates as the SNR grew. This pattern not only reaffirms the credibility and efficiency of the hybrid precoder and combiner's DDPG-based design but also highlights the system's adherence to anticipated theoretical models.

In parallel, a study focusing on BER relative to the count of RF chains, detailed in Fig. 26, identified a BER decline from 10^{-3} to 0 with the addition of more RF chains.

This trend matches the theoretical assumption that an increase in RF chains, contingent on precise channel estimation and the successful neutralization of inter-user disturbances, would naturally lead to BER diminishment, thus boosting overall system dependability.

The witnessed BER reduction with the rising number of RF chains validates the functional potency of the channel estimation carried out by ABPNN and the DHRR RIS structured through FHO. The practical outcomes presented, achieved through these dual evaluative standards, convincingly coincide with theoretical forecasts, thereby solidifying the proposed massive MIMO system's dependability and resilience.

In the realm of evaluating the bit error rate (BER) within communication systems, our proposed methodology exhibits significant advancements over existing strategies, particularly when contrasted with the two-timescale deep neural network (DNN) [33] approach utilized for hybrid precoding as shown in Figs. 27 and 28.

The two-timescale DNN method, while innovative, struggles with dynamic environmental shifts and the intricate demands of signal processing. Essentially, it's not always quick or responsive enough to handle the unpredictable nature of real-world communication channels. As a result, it often experiences a higher BER, impacting overall communication reliability.

Instead of reacting to errors after they occur, our system uses the ABPNN algorithm to predict and correct transmission errors by analysing critical factors like the angle of arrival (AoA), direction of arrival (DoA).

This pre-emptive stance helps maintain signal quality throughout the transmission process. What sets our approach apart is its ability to learn and adjust in real-time, a significant upgrade over the more static two-timescale DNN approach. Our findings,

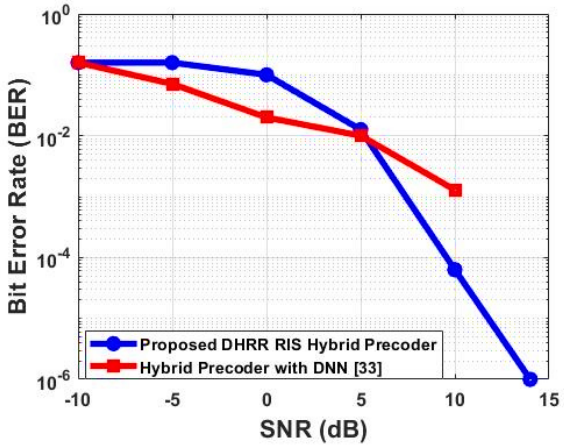

Figure. 27 BER vs SNR (comparative analysis)

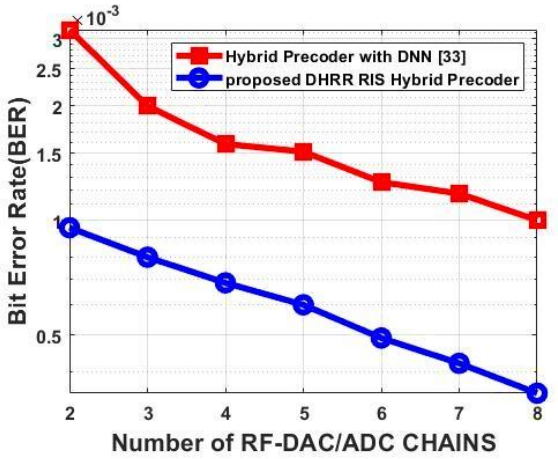

Figure. 28 BER vs varying RF-DAC/ADC chains (comparative analysis)

especially with 8 RF-DAC/ADC pairs and at an SNR of $10dB$ registering a BER of 0.0002, underscore the proposed model's merit in harmonizing enhanced channel estimation and minimized BER, fortifying its stance as a viable model for future communication systems' reliability and scalability.

11. Conclusion

This paper presents a comprehensive exploration into enhancing massive MIMO systems, beginning with the implementation of NniQ in low resolution ADCs/DACs to improve spectral and EE. The initial phase of the research established that NniQ-based systems could achieve SE comparable to that of systems utilizing UQ, with the added advantage of better EE. This approach laid the groundwork for subsequent advancements in the field.

Evolving further, the study embraced more complex Massive MIMO environments, integrating DHRR-RIS and advanced algorithmic paradigms. The introduction of RIS was strategic, addressing critical challenges such as excessive energy

consumption, channel estimation errors, and limitations in SE commonly associated with conventional MIMO systems. The innovation did not stop there; machine learning and deep learning algorithms were employed, optimizing processes like channel estimation, hybrid precoding and combining, and data clustering.

The sophistication introduced through DHRR-RIS, along with adaptive and deep reinforcement learning methodologies, marked a substantial enhancement in the system's operational intelligence. This intelligence was evident in improved CSI accuracy and the efficient handling of data streams, contributing to notable gains in overall system performance. The integration of non-uniform quantized 4-Bit DAC/ADCs and the strategic utilization of RIS components, especially when combined with artificial intelligence algorithms, optimized system reliability and signal integrity. This optimization translated into superior performance metrics, particularly in WSR and BER, as validated through rigorous simulation testing.

Conclusively, this research signifies a transformative approach in the design and implementation of Massive MIMO systems. By synergizing NniQ, RIS, and AI, the study has successfully demonstrated a methodology that surpasses traditional system limitations, setting a robust precedent for the development of more efficient, reliable, and high-capacity wireless communication networks. The results reaffirm the critical role of innovative, integrated technological strategies in shaping the future of wireless communications.

Conflicts of interest

The authors declare no conflict of interest.

Author contributions

The primary responsibilities and contributions of each author involved in this paper are as follows:

Girish Kumar N G: Involved in conceptualization, methodology development, software utilization, validation of results, formal analysis, investigation, resource accumulation, data curation, original draft preparation, and writing—review & editing.

Dr. M N Sree Ranga Raju: Contributed to visualization, offered supervision, and administered the project.

Both authors have read and agreed to the published version of the manuscript.

Acknowledgments

I extend my sincere gratitude to Prof. G. Sadashivappa, Professor & CoE, RVCE, Bangalore and Dr. Iven Jose, Professor and Dean, Christ University, Bangalore for their invaluable guidance and relentless support throughout my research journey. Their expertise has been instrumental in shaping this work. Additionally, I am thankful to my Institution, Bangalore Institute of Technology for providing the necessary resources and an intellectually stimulating environment that has been pivotal for the fruition of this research.

References

[1] C. Chen, Y. Wang, S. Aïssa, and M. Xia, "Low-Complexity Hybrid Analog and Digital Precoding for mmWave MIMO Systems", In: *Proc. of IEEE 31st Annual International Symposium on Personal, Indoor and Mobile Radio Communications*, pp. 1-6, 2020.

[2] L. Yang and W. Zhang, "Hybrid Precoding Design Achieving Fully Digital Performance for Millimeter Wave Communications", *Journal of Communications and Information Networks*, Vol. 3, No. 4, pp. 74-84, Dec. 2018.

[3] Q. Ding, Y. Deng, and X. Gao, "Spectral and EE of Hybrid Precoding for mmWave Massive MIMO With Low-Resolution ADCs/DACs", *IEEE Access*, Vol. 7, pp. 186529-186537, 2019.

[4] Y. Xiong, "Achievable Rates for Massive MIMO Relaying Systems with Variable-Bit ADCs/DACs", *IEEE Communications Letters*, Vol. 24, No. 5, pp. 991-994, May 2020.

[5] Q. Zhu, H. Li, R. Liu, M. Li, and Q. Liu, "Hybrid Beamforming and Passive Reflection Design for RIS-Assisted mmWave MIMO Systems", In: *Proc. of IEEE International Conference on Communications Workshops (ICC Workshops)*, Montreal, QC, Canada, pp. 1-6, 2021

[6] R. Schroeder, J. He, and M. Juntti, "Passive RIS vs. Hybrid RIS: A Comparative Study on Channel Estimation", In: *Proc. of 2021 IEEE 93rd Vehicular Technology Conference (VTC2021-Spring)*, Helsinki, Finland, pp. 1-7, 2021.

[7] A. W. Shaban, O. Damen, Y. Xin, and E. Au, "Statistically Aided Codebook-Based Hybrid Precoding for Millimeter Wave Channels", in *IEEE Access*, Vol. 8, pp. 101500-101513, 2020.

[8] Y. Huang, C. Liu, Y. Song, and X. Yu, "DFT codebook-based hybrid precoding for multiuser mmWave massive MIMO systems", *EURASIP J. Adv. Signal Process*, Vol. 11, 2020.

[9] A. Almradi, M. Matthaiou, P. Xiao, and V. F.

Fusco, "Hybrid Precoding for Massive MIMO With Low Rank Channels: A Two-Stage User Scheduling Approach", *IEEE Transactions on Communications*, Vol. 68, No. 8, pp. 4816-4831, Aug. 2020.

[10] W. Zhang, X. Xia, Y. Fu, and X. Bao, "Hybrid and full-digital beamforming in mmWave Massive MIMO systems: A comparison considering low-resolution ADCs", *China Communications*, Vol. 16, No. 6, pp. 91-102, June 2019.

[11] J. Liu, J. Dai, J. Wang, X. Yin, Z. Jiang, and J. Wang, "Achievable rates for full-duplex massive MIMO systems with low-resolution ADCs/DACs under imperfect CSI environment", *J Wireless Com Network*, 2018.

[12] J. Dai, J. Liu, J. Wang, J. Zhao, C. Cheng, and J. Y. Wang, "Achievable Rates for Full-Duplex Massive MIMO Systems with Low-Resolution ADCs/DACs", *IEEE Access*, Vol. 7, pp. 24343-24353, 2019.

[13] Q. Ding, Y. Lian, and Y. Jing, "Performance Analysis of Full-Duplex Massive MIMO Systems with Low-Resolution ADCs/DACs Over Rician Fading Channels", *IEEE Transactions on Vehicular Technology*, Vol. 69, No. 7, pp. 7389-7403, July 2020

[14] Q. Xu and P. Ren, "Secure Massive MIMO Downlink with Low-Resolution ADCs/DACs in the Presence of Active Eavesdropping", *IEEE Access*, Vol. 8, pp. 140981-140997, 2020.

[15] Y. Xiong, S. Sun, N. Wei, L. Liu, and Z. Zhang, "Performance Analysis of Massive MIMO Relay Systems with Variable-Resolution ADCs/DACs Over Spatially Correlated Channels", *IEEE Transactions on Vehicular Technology*, Vol. 70, No. 3, pp. 2619-2634, March 2021.

[16] H. Wang, C. Sun, J. Li, P. Zhu, D. Wang, and X. You, "Joint optimization of SE and EE with low-precision ADCs in cell-free massive MIMO systems", *Sci. China Inf. Sci*, Vol. 65, p. 152301, 2022.

[17] X. Zhang, T. Liang, K. An, G. Zheng, and S. Chatzinotas, "Secure Transmission in Cell-Free Massive MIMO With RF Impairments and Low-Resolution ADCs/DACs", *IEEE Transactions on Vehicular Technology*, Vol. 70, No. 9, pp. 8937-8949, Sept. 2021.

[18] J. Li, A. Wan, M. Zhou, J. Yuan, R. Yin, and L. Yang, "Downlink Analysis for the D2D Underlaid Multigroup Multicast Cell-Free Massive MIMO With Low-Resolution ADCs/DACs", *IEEE Access*, Vol. 10, pp. 115702-115715, 2022.

[19] Y. Zhang, D. Li, D. Qiao, and L. Zhang, "Analysis of Indoor THz Communication Systems with Finite-Bit DACs and ADCs", *IEEE Transactions on Vehicular Technology*, Vol. 71, No. 1, pp. 375-390, Jan. 2022.

[20] E. Balti and B. L. Evans, "Full-Duplex Massive MIMO Cellular Networks with Low Resolution ADC/DAC", In: *Proc. of GLOBECOM 2022 - 2022 IEEE Global Communications Conference*, Rio de Janeiro, Brazil, pp. 1649-1654, 2022.

[21] M. Zhou, Y. Zhang, X. Qiao, M. Xie, L. Yang, and H. Zhu, "Multigroup Multicast Downlink Cell-Free Massive MIMO Systems with Multiantenna Users and Low-Resolution ADCs/DACs", *IEEE Systems Journal*, Vol. 16, No. 3, pp. 3578-3589, Sept. 2022.

[22] I. S. Kim, M. Bennis, and J. Choi, "Cell-Free mmWave Massive MIMO Systems with Low-Capacity Fronthaul Links and Low-Resolution ADC/DACs", *IEEE Transactions on Vehicular Technology*, Vol. 71, No. 10, pp. 10512-10526, Oct. 2022.

[23] W. Zhang, J. Xia, and X. Bao, "Massive MIMO Systems with Low-Resolution ADCs: Achievable Rates and Allocation of Quantization Bits", *Wireless Communications and Mobile Computing*, Vol. 2023, Article ID 4012841, p. 12, 2023.

[24] J. Park, N. Lee, S. Hong, and Y. Jeon, "Learning from Noisy Labels for MIMO Detection with One-Bit ADCs", *IEEE Wireless Communications Letters*, Vol. 12, pp. 456-460, Mar. 2023

[25] L. Wen, H. Qian, Y. Hu, Z. Deng, and X. Luo, "One-bit Downlink Precoding for Massive MIMO OFDM System", *IEEE Transactions on Wireless Communications*, January 2023.

[26] Y. Lu, M. Hao, and R. Mackenzie, "Reconfigurable intelligent surface-based hybrid precoding for THz communications", *Intelligent and Converged Networks*, Vol. 3, No. 1, pp. 103-118, March 2022.

[27] H. Niu, Z. Chu, F. Zhou, C. Pan, D. W. Ng, and H. X. Nguyen, "Double Intelligent Reflecting Surface-Assisted Multi-User MIMO MmWave Systems with Hybrid Precoding", *IEEE Transactions on Vehicular Technology*, Vol. 71, pp. 1575-1587, 2021.

[28] C. Huang, Z. Yang, G. C. Alexandropoulos, K. Xiong, L. Wei, C. Yuen, Z. Zhang, and M. Debbah, "Multi-Hop RIS-Empowered Terahertz Communications: A DRL-Based Hybrid Beamforming Design", *IEEE Journal on Selected Areas in Communications*, Vol. 39, pp. 1663-1677, 2021.

[29] L. Dai, and X. Wei, "Distributed Machine Learning Based Downlink Channel Estimation for RIS Assisted Wireless Communications", *IEEE Transactions on Communications*, Vol. 70, pp. 4900-4909, 2022.

[30] J. Ye, S. Guo, and M. Alouini, "Joint Reflecting and Precoding Designs for SER Minimization in Reconfigurable Intelligent Surfaces Assisted MIMO Systems", *IEEE Transactions on Wireless Communications*, Vol. 19, pp. 5561-5574, 2019.

[31] Z. Zhou, N. Ge, Z. Wang, and L. H. Hanzo, "Joint Transmit Precoding and Reconfigurable Intelligent Surface Phase Adjustment: A Decomposition-Aided Channel Estimation Approach", *IEEE Transactions on Communications*, Vol. 69, pp. 1228-1243, 2020.

[32] Y. Wang, X. Chen, Y. Cai, and L. H. Hanzo, "RIS-Aided Hybrid Massive MIMO Systems Relying on Adaptive-Resolution ADCs: Robust Beamforming Design and Resource Allocation", *IEEE Transactions on Vehicular Technology*, Vol. 71, pp. 3281-3286, 2022.

[33] Q. Hu, Y. Cai, K. Kang, G. Yu, J. Hoydis, and Y. C. Eldar, "Two-Timescale End-to-End Learning for Channel Acquisition and Hybrid Precoding", *IEEE Journal on Selected Areas in Communications*, Vol. 40, pp. 163-181, 2022.

[34] Q. Sun, H. Zhao, J. Wang, and W. Chen, "Deep Learning-Based Joint CSI Feedback and Hybrid Precoding in FDD mmWave Massive MIMO Systems", *Entropy*, Vol. 24, 2022.

[35] X. Bao, W. Feng, J. Zheng, and J. Li, "Deep CNN and Equivalent Channel Based Hybrid Precoding for mmWave Massive MIMO Systems", *IEEE Access*, Vol. 8, pp. 19327-19335, 2020.

[36] X. Li, Y. J. Huang, W. Heng, and J. Wu, "Machine Learning-Inspired Hybrid Precoding for mmWave MU-MIMO Systems with Domestic Switch Network", *Sensors (Basel, Switzerland)*, Vol. 21, 2021.

[37] W. Ma, C. Qi, Z. Zhang, and J. Cheng, "Sparse Channel Estimation and Hybrid Precoding Using Deep Learning for Millimeter Wave Massive MIMO", *IEEE Transactions on Communications*, Vol. 68, pp. 2838-2849, 2020.

[38] K. M. Attiah, F. Sohrabi, and W. Yu, "Deep Learning for Channel Sensing and Hybrid Precoding in TDD Massive MIMO OFDM Systems", *IEEE Transactions on Wireless Communications*, 2022.

[39] Q. Lu, T. Lin, and Y. Zhu, "Channel Estimation and Hybrid Precoding for Millimeter Wave Communications: A Deep Learning-Based Approach", *IEEE Access*, Vol. 9, pp. 120924-120939, 2021.

[40] I. Kim and J. Choi, "Spatial Wideband Channel Estimation for mmWave Massive MIMO Systems with Hybrid Architectures and Low-Resolution ADCs", *IEEE Transactions on Wireless Communications*, Vol. 20, pp. 4016-4029, 2021.

[41] Y. Zhang, X. Dong, and Z. Zhang, "Machine Learning-Based Hybrid Precoding with Low-Resolution Analog Phase Shifters", *IEEE Communications Letters*, Vol. 25, pp. 186-190, 2021.

[42] X. Zhu, A. Koç, R. Morawski, and T. L. Ngoc, "A Deep Learning and Geospatial Data-Based Channel Estimation Technique for Hybrid Massive MIMO Systems", *IEEE Access*, Vol. 9, pp. 145115-145132, 2021.

[43] J. Shi, W. Wang, X. Yi, X. Gao, and G. Li, "Deep Learning-Based Robust Precoding for Massive MIMO", *IEEE Transactions on Communications*, Vol. 69, pp. 7429-7443, 2021.

[44] Q. Wang, K. Feng, X. Li, and S. Jin, "PrecoderNet: Hybrid Beamforming for Millimeter Wave Systems with Deep Reinforcement Learning", *IEEE Wireless Communications Letters*, Vol. 9, pp. 1677-1681, 2020.

[45] K. Wei, J. Xu, W. Xu, N. Wang, and D. Chen, "Distributed Neural Precoding for Hybrid mmWave MIMO Communications with Limited Feedback", *IEEE Communications Letters*, Vol. 26, pp. 1568-1572, 2022.

[46] J. Li, Y. Jiang, and L. Zhao, "Hybrid Precoding Design in Multi-User mmWave Massive MIMO Systems for BER Minimization", *IEEE Wireless Communications Letters*, 2023.